Sasol Advanced Fuels Laboratory

UNIVERSITY OF CAPE TOWN

Characterisation of the Autoignition Delay Behaviour of n-Heptane in the IQT™ Combustion Bomb Using CFD Modelling

Author:

Owen J. Metcalf

Supervised by:

Dr André Swarts, Dr Andy Yates and Dr Chris Meyer

A dissertation submitted to the Department of Mechanical Engineering, University of Cape Town, in partial fulfilment of the requirements for the degree of Master of Science in Engineering

Cape Town, South Africa
15 February 2007

Declaration

1. I know the meaning of plagiarism and declare that all the work in the document, save for that which is properly acknowledged, is my own.

2. I have used the Harvard convention for citation and referencing. Each significant contribution to, and quotation in this project from the works of other people has been attributed, and has been cited and referenced.

3. I have not allowed, and will not allow anyone to copy my work with the intention of passing it off as his or her own work.

Signature Signed by candidate

Abstract

Background

The ASTM D6890 (ASTM D6890, 2003) method predicts cetane numbers of diesel fuels based on the measured ignition delay in a combustion bomb (Ignition Quality Tester™). The device is calibrated using n-heptane as the reference fuel. When n-heptane was tested in the IQT™ device over a range of temperatures and pressures, the measured autoignition delay did not correlate with the chemical autoignition delay associated with a stoichiometric, homogeneous mixture as predicted by detailed chemical kinetic models. This is expected as the IQT™ test involves injection of fuel into a constant volume combustion chamber, and fuel sprays are inherently heterogeneous. It is, however, desirable to somehow cater for this inherent difference if the autoignition delay character of a fuel in the IQT™ is to be reconciled with the intrinsic autoignition delay characteristics predicted by detailed chemical kinetic modelling.

Objectives

This project involved an investigation to study and reconcile this discrepancy, using computational fluid dynamic (CFD) techniques to explore the physical conditions prevailing in the IQT™ device. Specifically, CFD was used to model fuel injection into the IQT™; this allowed a more accurate description of the fuel/air ratio and temperature history of the fuel inside the IQT™ combustion chamber than an assumption of global values. An empirical description of autoignition delay, developed by Yates et al. (2004), was then coupled to the CFD code: enabling the model to determine the progress of the fuel/air mixture to autoignition.

Results

In order to more accurately initialize the CFD model, measurements were taken of the temperature profile in the IQT™ combustion chamber. These measurements showed a significant level of variation in temperature along the length of the IQT™ axis. Although this does not have any effect on the accuracy of the IQT™ as a test method, it does mean that the fuel experiences a range of temperatures as it moves within the combustion chamber. This makes the CFD model of injection even more

relevant as a single temperature would be inappropriate to properly predict autoignition delay in the IQT™.

The CFD model was successful in predicting autoignition delays that were in good agreement with experimental data. This was especially true for n-heptane but results for iso-octane served to reinforce confidence in the technique. It was also found that the model was more accurate at higher temperatures, and hence shorter autoignition delays. This is not unexpected as the error associated with a numerical simulation is compounded over time. A model of 1-hexene autoignition was not as accurate, but this may have been due to a relative lack of literature data to support the empirical formulation for 1-hexene autoignition delay.

By using an inert particle, injected along with the fuel, to observe the conditions experienced by the fuel in the IQT™ over time, it was possible to record temperature and fuel/air equivalence ratio histories for various test conditions. This recorded data is accessible outside of the CFD environment and can be viewed and manipulated in Excel®. A recent study by Yates et al. (2007) made use of this data to reconcile the discrepancy between the conditions experienced by a fuel in the IQT™, and those used in the detailed chemical kinetic characterisation of a fuels intrinsic autoignition behaviour.

Conclusions

- The technique of using CFD modelling of fuel injection, in conjunction with the Yates model for autoignition delay, produced good agreement with experimental autoignition delay data from the IQT™. There are, however, conditions for which the model is best suited and they are as follows:

    - Short autoignition delays associated with high temperature and high cetane number fuels.
    - Fuels for which there is confidence in the chemical mechanism used for the detailed chemical kinetics, from which the coefficient of the empirical autoignition delay model are derived.

- The data recorded by the inert particle can be used to further understand the chemical reaction history of the autoignition of fuels in the IQT™ outside of the CFD environment, taking into account the temperature and fuel/air equivalence ratio history.

Table of Contents

List of Figures

List of Tables

Nomenclature

IQT™ - Ignition Quality Tester

CFD - Computational Fluid Dynamics

ID - Autoignition Delay

CN - Cetane Number

DCN - Derived Cetane Number

ASTM - American Society for Testing and Materials

UDF - User Defined Function

UDS - User Defined Scalar

τ - Autoignition delay

γ - Constant pressure correction factor

k - Fuel/air ratio correction factor

Φ - Fuel/air equivalence ratio (phi)

1 Introduction

A diesel fuel's propensity to auto-ignite is characterised by its cetane number. This is an important attribute of a diesel fuel, with higher cetane numbers offering desirable benefits in engine performance and emissions (Yates et al., 2004).

The benchmark method for determining the cetane number of a fuel is via the use of a single cylinder (CFR) test engine (ASTM D613, 2003). The method involves varying the compression ratio of the engine until the test fuel auto-ignites 2.41ms after injection. A blend of reference fuels is then formulated to match the performance of the test fuel at the same compression ratio, and the blend proportions define the cetane number of the test fuel.

A new cetane rating method has recently been developed, and extensively evaluated in the literature (Araldi et al., 1995; Allard et al., 1996; Allard et al., 1999), which is based on the Ignition Quality Tester (IQT™). The IQT™ is a combustion bomb apparatus in which the interval between the start of injection and the start of combustion (autoignition delay), at a defined temperature and pressure, correlates to a cetane value for the fuel. The relationship between autoignition delay (ID) and derived cetane number (DCN) is presented in Equation 1-1.

$$DCN = 83.99(ID - 1.512)^{-0.658} + 3.547 \qquad \text{(Eq 1-1)}$$

The difference in principle between the IQT method (fixed pressure and temperature) and the ASTM D613 method (variable pressure and temperature associated with the changing compression ratio) represents a subtle, but significant distinction. The IQT™ apparatus was approved by the American Society for Testing and Materials (ASTM) in 2003 as an alternative method for determining cetane number (ASTM D6890, 2003).

Although the ASTM D6890 method predicts cetane number reasonably accurately over a limited range (33 to 60 cetane numbers), it does not correctly predict the cetane value of primary and secondary reference fuel blends above 60 CN (Araldi et al., 1995; Allard et al., 1996; Yates et al., 2004). Yates et al. (2004) noted that the single calibration curve, relating ignition delay in the IQT™ to derived cetane number

(DCN) in the ASTM D613, was unable to properly describe the relationship between the two devices for all fuels. An alternative, more fundamental method of cetane prediction was investigated (Yates et al., 2004; Viljoen et al., 2005). This involved an empirical description of ignition delay (τ) as follows:

$$\tau_{overall} = \left\{\left(\tau_1 + \tau_2\right)^{-1} + \tau_3^{-1}\right\}^{-1} \quad \text{(Eq 1-2)}$$

Where

$$\tau_i = A_i p^{n_i} e^{B_i/T} \quad \text{(Eq 1-3)}$$

And T and p are the operating temperature and pressure respectively. τ_1 and τ_2 represent the low-intermediate temperature (<900K) behaviour, while τ_3 represents an alternative high temperature (>900K) reaction route. The nine coefficients ($A_{1\text{-}3}$, $n_{1\text{-}3}$, $B_{1\text{-}3}$) needed for Equation 1-2 were derived by fitting the empirical model to literature (Tao et al., 2000) and detailed chemical kinetic modelling data (Viljoen et al., 2005).

Although the proposed empirical model – hereafter referred to as the Yates model - is considered a good representation of the intrinsic, chemical autoignition delay behaviour of a stoichiometric mixture of n-heptane, the measured ignition delay in the IQT™ does not correlate well with such values. The relatively long ignition delays in the IQT™ result in a highly variable temperature history. This, coupled with the inherent heterogeneity of the air/fuel mixture, suggests the need for a better understanding of the conditions experienced by a fuel in the IQT™.

1.1 Initial Investigation

The first step in gaining the required understanding was to take a global look at the conditions in the IQT™. Rather than using the test temperature reported by the IQT™ and a fuel/air equivalence ratio of one, an effort was made to find more suitable values.

The first step was an attempt to resolve the discrepancy between the lean global fuel/air ratio in the IQT™, and the stoichiometric value used for the detailed chemical kinetic modelling. This was done by calculating the global fuel/air equivalence ratio in

the IQT™ and using this value to modify the autoignition delay predicted by the Yates model (Equation 1-2). The relationship between the autoignition delay under stoichiometric conditions ($\tau_{\varphi=1}$ given by Equation 1-2) and non-stoichiometric conditions (τ) was investigated by Londleni (2006) and has the following form:

$$\tau = \tau_{\phi=1} \cdot \phi^{k} \qquad \text{(Eq 1-4)}$$

In Equation 1-4 ϕ is the value of the fuel/air equivalence ratio under consideration, and k is the fuel/air equivalence ratio correction factor. It is clear that this equation has the effect of either increasing or decreasing the calculated autoignition delay depending on the values used for the fuel/air equivalence ratio and k.

The second step was based on the assumption of a heterogeneous temperature field inside the IQT™ combustion chamber, and involved solving for the average temperature experienced by a fuel in the IQT™. This was done using the Solver® tool in Excel® to derive a temperature that, when used in the Yates model, allowed autoignition delay predictions that matched the autoignition delays measured in the IQT™.

Had this initial investigation yielded a consistent relationship between the derived temperature and the test temperature reported by the IQT™, then the heterogeneous temperature field in the IQT™ could have been easily catered for. Unfortunately there was no such relationship that was applicable for all of the various test conditions under consideration. Furthermore it was also clear that the global fuel/air equivalence ratio, at the centre of the first step in the investigation, was an oversimplification that, while providing valuable insight at a later stage in the work, would not allow a sufficient description of the conditions experienced by a fuel in the IQT™.

1.2 CFD Modelling of Autoignition

It was proposed that Computational Fluid Dynamics (CFD) techniques could be used for the purposes of obtaining a more detailed understanding of conditions within the IQT™. Extensive use has been made of CFD to model n-heptane injection, autoignition and combustion.

Most of the studies that deal with autoignition and combustion use a combination of CFD and detailed chemical kinetics. Tao et al. (Tao et al., 1999; Tao et al., 2000; Tao et al., 2002) carried out several successful studies using this methodology; using CFD to simulate the spray into constant volume chambers and reduced chemical mechanisms to simulate autoignition and combustion. Gustavsson et al. (2004) used similar techniques to investigate three-dimensional modelling of HCCI combustion, again with good results.

The problem with a CFD-Chemical kinetic model is that it requires vast computational resources and time. Ali et al. (2003) carried out a study in an attempt to improve the efficiency of this method. It was found that by systematically reducing the number of chemical mechanisms and using parallel processing, they were able to bring computational time down significantly, while still maintaining good agreement with the more detailed chemical mechanisms. Although the improvements achieved by Ali et al were useful, the method of improvement involved significant hardware costs.

It is believed that proper implementation of the Yates model as a simplified description of the reaction route may prove to be a simpler way to reduce computational time and resources while still accurately predicting autoignition.

Realistic spray simulation has also been investigated. Correct spray penetration and structure are necessary for accurate combustion apparatus modelling. Barroso et al. (2003) carried out an extensive parametric study of evaporating diesel sprays. The goal of the study was to establish the sensitivity of spray simulation to various modelling variables such as grid structure and turbulence initialization. The results of the study were verified using detailed shadowgraphy and Phase Doppler Anemometry. This sensitivity study served to eliminate some of the uncertainty involved in successfully modelling diesel injection and support the used of CFD to model injection in the IQT™.

1.3 Project Objectives

The specific objectives of the project were as follows:

- To gain an understanding of the reason for the discrepancy between calculated - using homogenous temperature, pressure and fuel/air ratio assumptions - and measured autoignition delay in the IQT™.
- To use this understanding to adapt the Yates model to characterise the autoignition delay behaviour of fuels in the IQT™ specifically.

In order to achieve these objectives the following steps were taken:

- The operating conditions in the IQT™ were measured in greater detail.
- The measured operating conditions were used as the initial conditions in a CFD simulation of fuel injection into the IQT™.
- The Yates model was incorporated into the CFD model to determine the onset of autoignition.
- The temperature and fuel/air ratio history of the fuel was captured for various IQT™ operating conditions and used to adapt the Yates model to better describe autoignition delay behaviour in the IQT™.

1.4 Report Layout

This report details the work done to achieve the project objectives as well as the results thereof. The remainder of this report has the following layout:

- **Theoretical Background:** This chapter is intended to give the reader a brief introduction to the more technical concepts central to this work. Specifically it aims to provide a basic understanding of computational fluid dynamics (CFD) as well as the process involved in, and the modelling of, autoignition.

- **Literature Review:** In this chapter the reader is presented with a summary of the ideas that form the theoretical basis for the approach taken to meet the project objectives. A logical sequence of ideas is presented, based on a study of the

literature, which results in a preferred modelling philosophy and specific attention to the method in which to implement it.

- **Modelling Methodology:** This chapter begins with a broad description of the modelling philosophy used in this project. This is followed by a step-by-step presentation of the process of modelling the IQT™ for the prediction of autoignition and fuel history.

- **Results:** This chapter presents the results of the project, including the results of temperature measurements taken in the IQT™ and those of the CFD autoignition model.

- **Analysis of Results:** As the name suggests, this chapter involves an analysis and discussion of the results presented in the previous chapter. The aim is to objectively examine the results and extract useful ideas and conclusions, as well as to attempt to explain anomalous results and failings of the CFD autoignition model.

- **Conclusions:** The findings of the study are summarised in this chapter.

- **Recommendations:** This chapter contains recommendations based on the results and conclusions of the preceding chapters.

2 Theoretical Background

2.1 CFD Fundamentals

Computational Fluid Dynamics (CFD) is the analysis of physical phenomena, involving flow, with the use of a computer simulation (Versteeg et al., 1995). There are three parts to any CFD package; the pre-processor, the solver and the post-processor. A brief description of each part is as follows:

- **Pre-processor:** This is basically the setup stage of a CFD model. Here the geometry of the domain of interest is defined and sub-divided. The sub-division consists of the generation of a grid of small computational cells.

  Following the grid generation the user is required to define the fluid properties, the initial or boundary conditions and what phenomena need to be modelled.

- **Solver:** This is where the transport equations are solved in accordance with the user inputs, defined in the pre-processor. The process of solving fluid flow involves integration of the governing equation of flow. By sub-dividing the geometry into small computational cells it is possible to perform the integration over small volumes and simplify it by a process known as discretisation.

- **Post-processor:** This is where the user is able to see the solution generated by the solver. Post-processing includes the ability to export data for external manipulation, to view graphical representations of the numerical data and even to animate simulations.

Transport Equation

Versteeg et al. (1995) provides the following form of the general transport equation for a flow variable ϕ of a Newtonian fluid, in a small fluid element (a computational cell):

$$\frac{\partial(\rho\phi)}{\partial t} + div(\rho\phi\vec{u}) = div(\Gamma grad\phi) + S_\phi \qquad \text{(Eq 2-1)}$$

The first and second terms on the left hand side of Equation 2-1 are the rate of change and convective terms respectively. The right hand side gives the diffusive term followed by the source term. This equation is described by Versteeg et al. (1995) as follows:

[Rate of increase of ϕ of fluid element] + *[Net rate of flow of ϕ out of fluid element]* = *[Rate of increase of ϕ due to diffusion]* + *[Rate of increase of ϕ due to sources]*

Appropriate assignment of the value of ϕ and the diffusion coefficient Γ allow this general equation to be applied to the solution of a variety of flow variables. An example of the application of the general transport equation is shown below for the solution of temperature change due to steady-state conduction (diffusion) and heat loss.

$$div(kgradT) + q = 0 \qquad \text{(Eq 2-2)}$$

In the above equation the flow variable is temperature T (K), the diffusion coefficient is the thermal conductivity k (W/mK) and the source term S_T is replaced by the heat loss q (W/m^3). The other terms are zero as this example is of a steady-state diffusion problem which has no time dependant change and no convection.

In order to solve the general transport equation for a fluid element it is necessary to integrate over the computational cell that makes up the fluid element. Equation 2-1 is thus integrated as follows:

$$\int_{CV} \frac{\partial(\rho\phi)}{\partial t} dV + \int_{CV} div(\rho\phi\vec{u}) dV = \int_{CV} div(\Gamma grad\phi) dV + \int_{CV} S_\phi dV \qquad \text{(Eq 2-3)}$$

The volume integral in Equation 2-3 can be simplified using Gauss' divergence theorem and the simplified form is as follows:

$$\frac{\partial}{\partial t}\left(\int_{CV} \rho\phi dV\right) + \int_A \vec{n}.(\rho\phi\vec{u}) dA = \int_A \vec{n}.(\Gamma grad\phi) dA + \int_{CV} S_\phi dV \qquad \text{(Eq 2-4)}$$

The diffusion and convection terms have now been reduced to a description of net flux across the cell boundaries. Versteeg et al. (1995) states Equation 2-4 in words as follows:

[Rate of increase of ϕ] **+** *[Net rate of decrease of ϕ due to convection across the boundaries]* **=** *[Rate of increase of ϕ due to diffusion across the boundaries]* **+** *[Net rate of creation of ϕ]*

For an unsteady simulation there is a time dependence that must be catered for by integration with respect to time. The general unsteady solution of a flow variable ϕ, for a Newtonian fluid is presented by Versteeg et al. (1995) as follows:

$$\int_{\Delta t}\frac{\partial}{\partial t}\left(\int_{CV}\rho\phi dV\right)dt+\int_{\Delta t}\int_{A}\vec{n}.(\rho\phi\vec{u})dAdt=\int_{\Delta t}\int_{A}\vec{n}.(\Gamma grad\phi)dAdt+\int_{\Delta t}\int_{CV}S_{\phi}dVdt \quad \text{(Eq 2-5)}$$

Discretisation

The control volume integration described above is a method of solving the transport equation that is specific to the Finite Volume Method (FVM) of CFD. This is the most common method of solving CFD problems and involves the division of the fluid domain into small control volumes (computational cells) over which the transport equation can be integrated.

In order to perform the integration it is necessary to approximate the integral as a system of algebraic equations. This process is known as discretisation. An example taken from *An Introduction to Computational Fluid Dynamics* (Versteeg et al., 1995) will serve to illustrate the concept of discretisation for the solution of one-dimensional diffusion by the finite volume method:

The general transport equation for one-dimensional steady state diffusion is as follows:

$$\frac{d}{dx}\left(\Gamma\frac{d\phi}{dx}\right)+S=0 \quad \text{(Eq 2-6)}$$

This example deals with the solution of the value of ϕ at the node in the centre of a control volume where the control volume is not on the boundary of the fluid domain.

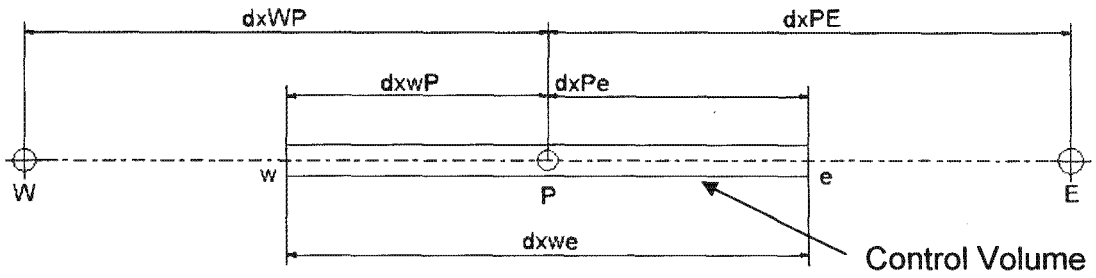

Figure 2-1. Control volume layout.

Figure 2-1 shows the control volume under consideration. *P* is the node for which the solution is being sought. *W* and *E* are the nodes at the centre of the cells to the west and east respectively. The small *w* and *e* denote the western and eastern boundaries of the control volume. This is a node centred formulation which means that the node is always halfway between the cell boundaries, such that the distance from *w* to *P* is the same as the distance from *P* to *e*. As a simplification, the grid in this example is uniform so that the distance from *P* to *E* (dx_{PE}) is the same as the distance from *W* to *P* (dx_{WP}) and twice the distance from a node to a boundary.

In order to solve the transport equation the volume integral of Equation 2-6 is approximated as a system of linear equations. In order to do this it is necessary to know something about the values of the flow variable ϕ on the control volume boundaries, as these are the points between which the integration is applied as follows:

$$\int_{CV} \frac{d}{dx}\left(\Gamma \frac{d\phi}{dx}\right) dV + \int_{CV} S dV = \left(\Gamma A \frac{d\phi}{dx}\right)_e - \left(\Gamma A \frac{d\phi}{dx}\right)_w + \bar{S}\Delta V = 0 \qquad \text{(Eq 2-7)}$$

It is the approximation of values at the control volume boundaries that is referred to as discretisation. The discretisation scheme used for this problem is known as *central differencing*. As the name suggests, *central differencing* linearly approximates the value at a boundary based on known nodal values on either side of it. For a uniform

grid, as used in this example, this means that the value at the boundary will be exactly half way between the values of the nodes to either side of it. The diffusion coefficients are defined as follows:

$$\Gamma_w = \frac{\Gamma_W + \Gamma_P}{2} \quad \text{(Eq 2-8)}$$

$$\Gamma_e = \frac{\Gamma_P + \Gamma_E}{2} \quad \text{(Eq 2-9)}$$

The other part of the diffusive flux term $\frac{d\phi}{dx}$, is simply the rate of change of the flow variable at the boundary and if a constant gradient is assumed between nodes then the diffusive flux terms can be defined as follows:

$$\left(\Gamma A \frac{d\phi}{dx}\right)_e = \Gamma_e A_e \left(\frac{\phi_E - \phi_P}{\delta x_{PE}}\right) \quad \text{(Eq 2-10)}$$

$$\left(\Gamma A \frac{d\phi}{dx}\right)_w = \Gamma_w A_w \left(\frac{\phi_P - \phi_W}{\delta x_{WP}}\right) \quad \text{(Eq 2-11)}$$

The source term can also be approximated linearly:

$$\overline{S}\Delta V = S_u + S_P \phi_P \quad \text{(Eq 2-12)}$$

In the equation above the source term is made up of two components, a term that is constant throughout the domain (Su) and one that is dependant on the value of the flow variable under consideration ($Sp\phi$). An example of the first would be heat loss to the surroundings where a uniform temperature difference, between the fluid and the surroundings, is present throughout the domain; such a heat loss could be modelled as a constant. An example of the second term is heat loss where the temperature difference between the fluid and the surroundings is not consistent throughout the domain; the magnitude of this heat loss would need to be evaluated at every nodal position.

This procedure can be carried out for every control volume in the fluid domain. It will result in the formation of a matrix of expressions where the values at each node are dependant on the values of the surrounding nodes.

Clearly this is not sufficient to solve the problem as up to this point only variables have been used to derive a co-dependence. To close the solution loop, and allow the iterative solution of all of the nodal values it is necessary to provide boundary conditions. At the fluid boundary there is a special treatment with regards to the discretisation. It is not necessary to interpolate for the value of a control volume boundary if that boundary is on the fluid domain boundary. This is because the values at the fluid domain boundaries defined by the user and are therefore known. In this way the co-dependence on neighbouring nodal values is not present on at least one boundary of a control volume on the fluid domain boundary.

An iterative technique allows the effect of the boundary conditions to "spread" through the fluid domain via the co-dependence of one nodal value on that of its neighbour. This "spreading" will happen until a steady state condition is reached. At this point the problem is solved.

The example given above is of the most basic type - one-dimensional, steady state diffusion – but it is effective in illustrating to concept of discretisation. The discretisation scheme used was *central differencing,* but a number of other schemes exist that are more appropriate for more complex problems.

Discrete phase modelling

Up to this point an Eulerian approach has been considered, where the computational mesh, making up the control volumes, is stationary with respect to the fluid domain. The fluid flow is then modelled as passing through the stationary mesh via convective or diffusive flux.

A second approach is employed for the modelling of discrete particles. In this approach the discrete particle variables are stored at the position of the discrete particle itself. In a way the discrete particle is like a moving node that has a variable level of interaction with the nodes in the Eulerian mesh around it. For example the user can decide whether to model heat transfer between the discrete (Lagrangian) and continuous (Eulerian) phases. Similarly by allowing a particle to vaporise and/or boil the user is activating mass transfer between the discrete and continuous phases, as the vapour will be treated in an Eulerian fashion.

The discrete phase modelling capability of commercial CFD packages such as FLUENT® - which is used for the modelling in this project - is what allows the modelling of fuel injections and other particle phenomena, and plays a central role in this project.

User Defined Function (UDF)

Finally, for the purposes of this project it was necessary to make use of User Defined Functions (UDFs). UDFs are algorithms, written in the C++ language, that allow the user to access the more advanced functionality of FLUENT®. It is possible, for example, to define non-standard functions for the treatment of flow behaviour, to perform difficult initialisations or to access solver variables at the end of a time step. These are just a few examples of what UDFs can be used for but there are in fact many more.

The important thing to understand about UDFs is that they provide a very wide range of functionality, beyond that which is offered by the graphical user interface (GUI) of the pre-processor. The GUI consists of a set of menus for accessing various functions of the CFD package. For example it allows users to select from various preset options, input properties, save and read data and issue predefined instructions. However, as comprehensive as the list of predefined options and settings are, they cannot possibly cover the full capability of a CFD package such as FLUENT®. When it is necessary to do something that is not possible via the GUI, the user must make use of UDFs.

2.2 Autoignition Modelling

The autoignition process

The traditional understanding of autoignition chemistry sees the chemical processes, leading to autoignition, divided into three regimes. This division is based roughly on three temperature ranges and the dominant reactions in each. Curran, Pitz and Westbrook (1998; 2002) have carried out extensive analysis of these processes and they are summarised as follows:

- The low temperature or cool flame regime, between 800K and 850K, is mainly associated with the decomposition of Ketohydroxide species leading to rapid chain branching and a sudden heat release.

- The low-intermediate regime (<900K) is dominated by Alkyl radical addition to molecular Oxygen; $R\bullet + O_2 \Leftrightarrow RO\bullet_2$. The activation energy for the addition reaction is taken as zero while the reverse reaction has relatively high activation energy of ~30Kcal/mol (Curran et al., 1998). This results in the equilibrium constant for this reaction being strongly dependant on temperature. At low temperatures the addition reaction proceeds rapidly while at high temperatures the dissociation reaction is favoured, rapidly reducing the concentration of $RO\bullet_2$, thereby shutting off the low temperature branching reactions and reducing the reaction rate and heat release. This results in the Negative Temperature Coefficient (NTC) region shown in Figure 2-2, with increasing temperature resulting in increasing autoignition delay (ID).

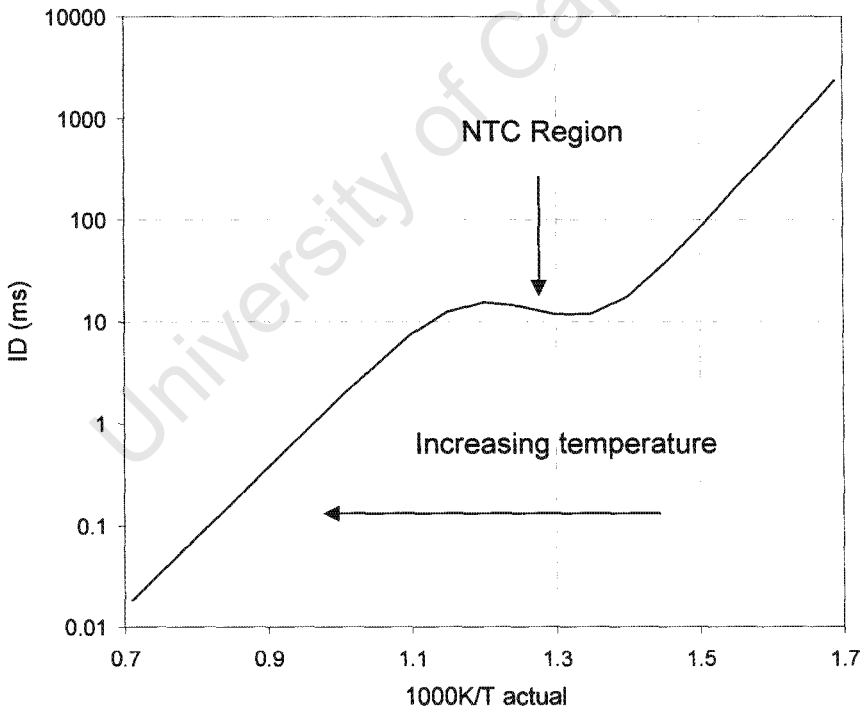

Figure 2-2. Typical autoignition delay map over a range of temperatures.

Pressure influences the equilibrium of the reaction as indicated by the La Chatelier principal; as the pressure is increased the equilibrium temperature lowers. Westbrook et al. (1998) found that a two-fold increase in pressure shifted the equilibrium point by 50 degrees.

- Above 900K the reaction is driven increasingly by the decomposition of hydrogen peroxide. The activation energy required for this reaction is high (~45Kcal/mol Westbrook et al., 1998) so the reaction is quite slow in the range 800K to 1000K. Thereafter the decomposition proceeds rapidly and, once beyond the NTC region, any increase in temperature will be associated with a shorter autoignition delay.

Detailed chemical modelling

Any attempt to predict autoignition numerically requires some degree of simplification. The least simplification is available when using detailed chemical kinetic modelling. This method consists of numerically performing the thousands of possible reactions on the path to autoignition. This method was evaluated by Viljoen et al. (2005) and was found to produce good agreement with literature data. It was found that detailed chemical kinetic modelling was able to accurately predict the autoignition behaviour of a fuel as long as sufficient data is available with respect to the chemical mechanisms leading to autoignition.

It is possible to use this modelling approach in conjunction with a CFD package to model autoignition of diesel sprays (Tao et al., 1999; Tao et al., 2000; Tao et al., 2002; Gustavsson et al., 2004), where the physical characteristics of the fuel/air interaction are as important as the chemical mechanisms. This approach is, however, computationally demanding and time consuming. It is possible to use parallel processing and/or reduced chemical mechanisms to reduce the time to result (Ali et al., 2003), but the former involves significant hardware expenses while the latter may compromise the ability of the model to resolve phenomena such as NTC behaviour.

Simplified empirical description

A simpler method of predicting autoignition delay involves using an Arrhenius expression to describe instantaneous reaction rate as a function of various fuel and operating parameters. Livengood and Wu (1955) defined the onset of autoignition as the time at which the integral of the reaction rate with respect to time reached a value of unity.

The inverse of the reaction rate is the autoignition delay, and the following empirical descriptions of this quantity are of particular importance in this project:

- Douaud and Eyzat (1987) used a single Arrhenius equation to describe autoignition delay:

$$\tau = 17.68(ON/100)^{3.402} p^{-1.7} e^{(3800/T)} \quad \text{(Eq 2-13)}$$

Where τ is the autoignition delay in milliseconds, p is the absolute pressure in atmospheres, ON is the octane number of the fuel and T is the temperature in Kelvin.

It is clear that this equation only allows for single stage behaviour and cannot possibly describe the behaviour of a fuel accurately over a range of temperatures encompassing the low, high and intermediate temperature regimes.

- Yates et al. (2004) proposed a new empirical definition of autoignition delay also based on the Arrhenius equation. This expression involves the coupling of three Arrhenius equations as follows:

$$\tau_{overall} = \left\{(\tau_1 + \tau_2)^{-1} + \tau_3^{-1}\right\}^{-1} \quad \text{(Eq 2-14)}$$

Where

$$\tau_i = A_i p^{n_i} e^{B_i/T} \quad \text{(Eq 2-15)}$$

And T and p are the temperature in Kelvin and the pressure in bar respectively. The nine coefficients ($A_{1\text{-}3}$, $n_{1\text{-}3}$, $B_{1\text{-}3}$) were derived by fitting the empirical model to literature (Tao et al., 2000) and detailed chemical kinetic modelling data (Viljoen et al., 2005).

It is clear that, as long as data is available for deriving the coefficients A, B and n, the Yates model will be able to accurately describe the autoignition delay behaviour of a fuel in each of the three temperature regimes. τ_1 and τ_2 describe the sequential reactions of the low and intermediate temperature regimes while τ_3 describes an alternative high temperature reaction route representing the

increasingly dominant hydrogen peroxide decomposition. Figure 2-3 shows a comparison between the Yates model and the Douaud model for iso-octane over a range of temperatures. Literature data is included as a reference.

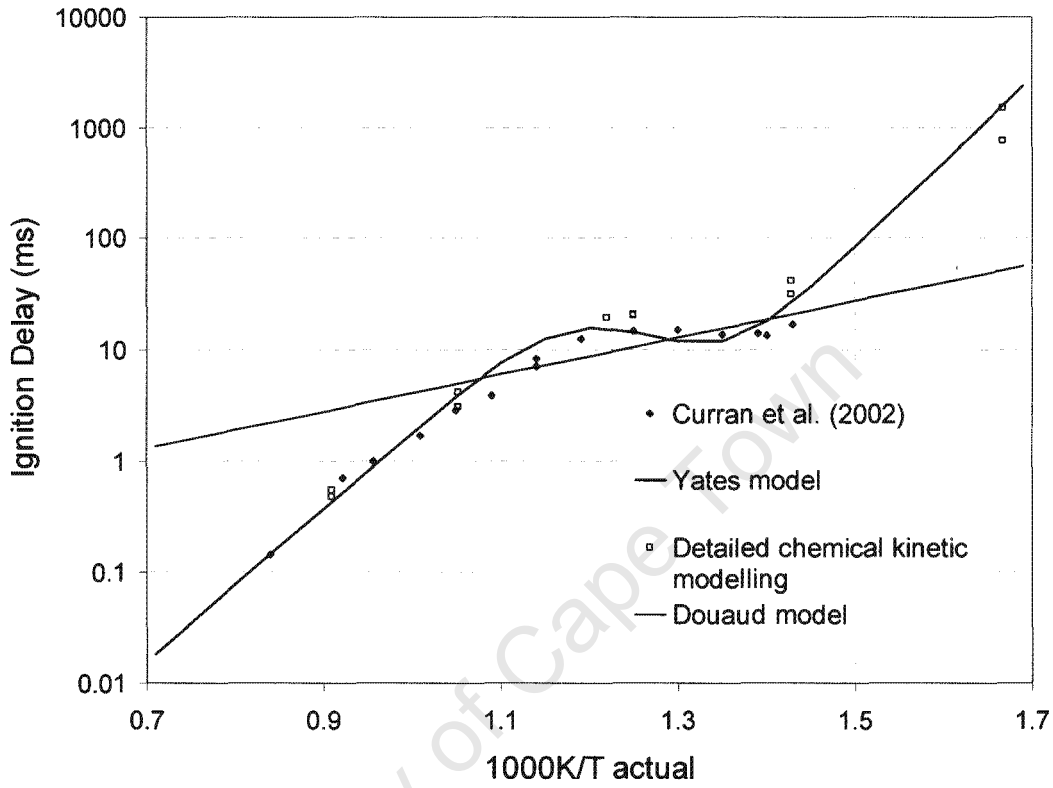

Figure 2-3. Comparison between the Yates and Douaud models for prediction of autoignition delay of iso-octane.

- An improved empirical model has since been developed by Yates et al. (2007) that is fitted to the same literature data as before and updated chemical kinetic data (Viljoen et al., 2007). It provides a more physically descriptive depiction of the ignition delay behaviour of the fuel. The new model is formulated as follows:

$$\tau_{overall} = (\tau_1 + \tau_2) \qquad \text{(Eq 2-16)}$$

Where

$$\tau_1 = p^{n_1} e^{(\ln A_1 + B_1/T)} \left(1 - e^{(-B_2 \Delta T/\gamma T^2)}\right) \qquad \text{(Eq 2-17)}$$

And

$$\tau_2 = p^{n_2} e^{(\ln A_2 + B_2/(T + \Delta T/\gamma))} \qquad \text{(Eq 2-18)}$$

And

$$\Delta T = \left(C_1 T + C_2 p^m + \sqrt{\left(C_1 T + C_2 p^m\right)^2 - C_0 C_1} \right) / 2 \qquad \text{(Eq 2-19)}$$

This new model represents an empirical description of the high-temperature autoignition reaction following a period of exposure to the initial temperature T, and a sequential exposure to a higher temperature $T+\Delta T$, representing the post cool-flame environment. The temperature development depicted by this model is shown in Figure 2-4.

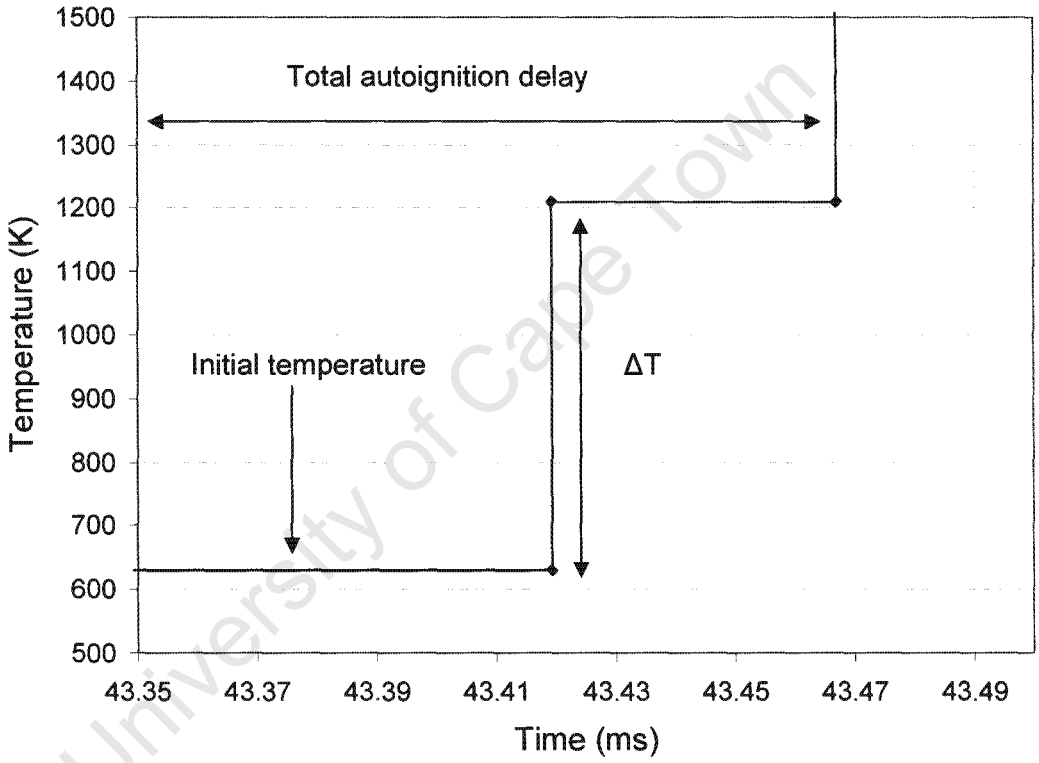

Figure 2-4. Cool flame temperature rise as modelled by Viljoen using detailed chemical kinetics.

The chemical kinetic modelling was performed for homogeneous, constant volume conditions and for this condition a rise in temperature such as ΔT would result in a corresponding rise in pressure. In a situation of spray injection the increase in temperature due to cool flame reaction would be very localised and ongoing, and hence have negligible effect on the pressure. This reduced effect is simulated by the use of the γ term found in Equations 2-17 and 2-18.

The γ term is derived by relating the temperature rise (ΔT in Equation 2-19) at constant volume – as modelled by the detailed chemical kinetics - to that at

constant pressure – as seen in the IQT™ - while maintaining changes in internal energy. This relationship is shown in Equation 2-20.

$$c_v \Delta T_{cv} = c_p \Delta T_{cp} \qquad \text{(Eq 2-20)}$$

In Equation 2-20 ΔT_{cv} is the temperature rise at constant volume and ΔT_{cp} is the temperature rise at constant pressure, while c_v and c_p are the respective specific heats. This results in the following:

$$\Delta T_{cp} = \frac{c_v}{c_p} \Delta T_{cv} \qquad \text{(Eq 2-21)}$$

If the ratio of specific heats is presented as follows:

$$\gamma = \frac{c_p}{c_v} \qquad \text{(Eq 2-22)}$$

Then when substituting back into Equation 2-21, the following relationship emerges:

$$\Delta T_{cp} = \frac{\Delta T_{cv}}{\gamma} \qquad \text{(Eq 2-23)}$$

Equation 2-23 shows the role played by γ in Equations 2-17 and 2-18. It is used to convert the constant volume temperature rise, given by Equation 2-19, to a constant pressure value, more representative of the behaviour in the IQT™.

- As part of a study by Londleni (2006), a method was derived whereby the models proposed by Yates et al. (Equations 2-14 and 2-16) could be applied to non-stoichiometric problems. This was done by an analysis of detailed chemical kinetic modelling data and the following result was achieved:

$$\tau = \tau_{\phi=1} . \phi^k \qquad \text{(Eq 2-24)}$$

Where $\tau_{\phi=1}$ is the value of the autoignition delay under stoichiometric conditions, ϕ is the fuel/air equivalence ratio and k is the fuel/air equivalence ratio correction factor. The work was done for fuels with octane numbers between 0 (n-heptane) and 100 (iso-octane), and for equivalence ratios between 0.2 and 2.5. Londleni (2006) proposed a value of -0.77 as appropriate for k.

It is important to clarify that in Equation 2-24 ϕ is used to indicate the fuel/air equivalence ratio, not a general flow variable as in Section 2.1. From this point onwards ϕ will *always* refer to the fuel/air equivalence ratio, the alternative use in Section 2.1 was maintained to avoid confusion should the reader wish to reference Versteeg et al. (1995).

3 Literature Review

3.1 Cetane Number Determination

Cetane number is a property associated with any diesel fuel. Like octane number, for petrol, cetane number is an indicator of how a particular fuel can be expected to perform in an engine. Unlike octane number, which indicates the resistance of a petrol fuel to autoignition, cetane number is an indicator of the propensity of a diesel fuel to auto-ignite. Since a diesel engine relies on the autoignition of fuel for combustion, it follows that a high cetane number is desirable.

High cetane number fuels will auto-ignite more readily allowing benefits such as easier cold starting, lower emissions (less unburned fuel) and higher power output (Yates et al., 2004). A high cetane number is therefore a valuable property of a diesel fuel, making the correct determination of cetane number important.

ASTM D613 CFR engine

The CFR test engine (ASTM D613, 2003) is the benchmark method for determining the cetane number of a fuel. The test fuel is run in a single cylinder, indirect injection engine and the compression ratio of the engine is varied, by changing the pre-chamber volume, until the fuel auto-ignites 2.41ms after injection. The compression ratio is then kept constant and a blend of reference fuels is made up to match the autoignition performance of the test fuel. The blend proportions directly define the cetane number of the test fuel. Details of this method are as follows:

- Operating conditions[i]:
  - Engine speed: 900rpm
  - Inlet temperature: 65.56 °C
  - Start of injection (SOI): 13° Before Top Dead Centre (BTDC)
  - Fuel flow rate: 13ml/min
  - Required start of combustion: TDC (13 or 2.41ms autoignition delay)

[i] Online, available: http://www.me.iastate.edu/biodiesel/Pages/biodiesel17.html

- Reference fuels:
  - n-Hexadecane (n-Cetane) – Cetane number of 100
  - Heptamethylnonane (HMN) – Cetane number of 15

- Cetane number definition:
  - Cetane number = %n-cetane + 0.15%HMN (Eq 3-1)

ASTM D6890 Ignition Quality Tester (IQT™)

A new method for cetane number determination has recently been developed which is based on the Ignition Quality Tester (IQT™). The IQT™ is a combustion bomb apparatus in which the interval between the start of injection and the start of combustion (autoignition delay), at a defined temperature and pressure, correlates to a cetane value for the fuel. The IQT™ apparatus has been extensively evaluated in the literature (Araldi et al., 1995; Allard et al., 1996; Allard et al., 1999), and it was approved by the American Society for Testing and Materials (ASTM) in 2003 as an alternative method for determining cetane number (ASTM D6809, 2003). The details of the method are as follows:

- Operating conditions (Advanced Engine Technology, 2003):
  - Standard test temperature: 545 ± 30°C
  - Standard operating pressure: 2.137 ± 0.007 MPa
  - Injection Nozzle coolant temperature: 50 ± 4°C
  - Combustion chamber pressure sensor temperature: 130 ± 20°C

- Reference fuels:
  - n-Heptane – Calibration Reference Fuel: required ignition delay of 3.78ms

- Cetane number definition:
  - Derived Cetane Number (DCN) = $83.99(ID-1.512)^{-0.658}+3.547$ (Eq 3-2)
    (ID is the autoignition delay in milliseconds)

- Test sequence: The user controls the test temperature indirectly by varying the setpoint temperature. The test temperature that must be kept within the range 545 ± 30°C. Once the required test temperature is achieved the automated test sequence begins. This consists of 15 pre-injections and 32 recorded injections.

Before each injection the chamber is charged with fresh air and a delay is included to allow the charge air to be heated by the chamber walls. At the end of the test a detailed report is printed containing various parameters recorded at each injection. These include the autoignition delay, derived cetane number and test temperature. For an example of a detailed report see Appendix 3.

Figure 3-1 contains an excerpt from the IQT™ user manual and shows the layout of the IQT™, indicating the points where various temperatures are measured.

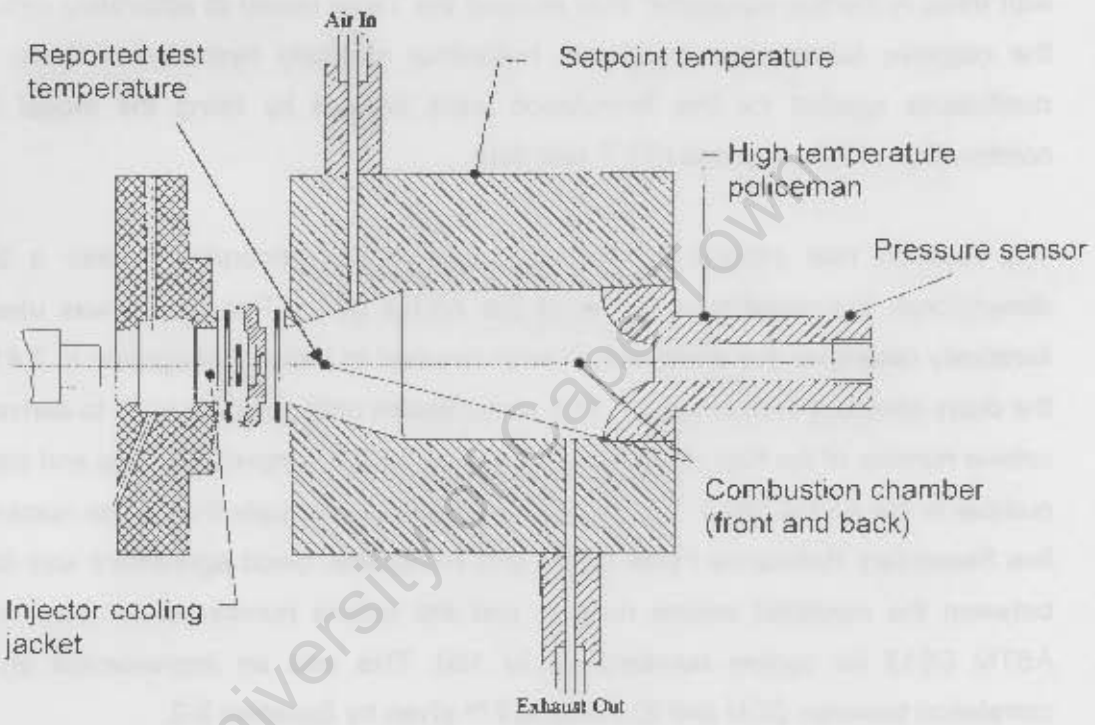

Figure 3-1. IQT™ layout with temperature measurement points indicated.

3.2 Relating the ASTM D613 CFR Engine and the IQT™

Yates et al. (2004) published a paper - *Understanding the Relationship between Cetane Number and Combustion Bomb Ignition Delay Measurements* - that tried to understand the relationship between these two methods.

It was found that the single calibration curve (Equation 3-2), relating autoignition delay in the IQT™ to the Derived Cetane Number (DCN) in the ASTM D613, was unable to properly determine the cetane number of all fuels. This is because of the

different responses of different fuels to changes in temperature and pressure. A more fundamental description of the autoignition behaviour of fuels was required. An empirical formulation was developed based on the methods employed by Douaud et al. (1987) and Livengood and Wu (1955). Douaud and Eyzat (1987) used a single Arrhenius equation to describe the autoignition delay of a particular fuel. Livengood and Wu (1955) developed a method to determine the onset of autoignition under changing conditions; where autoignition occurs when the value of the integral of the reaction rate (the inverse of the autoignition delay) with respect to time reaches unity. Yates et al. (2004) improved on this methodology by describing the autoignition delay with three Arrhenius equations. This allowed the Yates model to accurately describe the negative temperature coefficient behaviour of many hydrocarbon fuels. The coefficients needed for this formulation were derived by fitting the model to a combination of literature and IQT™ test data.

The reaction rate integral of the Yates model was incorporated into a zero-dimensional, thermodynamic model of the ASTM D613. This model was used to iteratively determine the compression ratio required to initiate autoignition in 2.41ms; the delay specified in the method. This compression ratio could be used to derive the cetane number of the fuel; via the relationship between compression ratio and cetane number in the ASTM D613. This method was used to evaluate the cetane number of five Secondary Reference Fuels (SRF) and n-heptane. Good agreement was found between the modelled cetane number and the cetane number determined in the ASTM D613 for cetane numbers up to 100. This was an improvement on the correlation between DCN and ID in the IQT™ given by Equation 3-2.

While this methodology is useful, it requires IQT™ test data in order to solve for the various Arrhenius coefficients. When using coefficients derived solely from literature and detailed chemical kinetic modelling, the autoignition delay predicted by the Yates model does not agree with the test data from the IQT™. If these coefficients are assumed to be a good description of the intrinsic chemical behaviour of the fuel, then the discrepancy must be due to physical differences between the conditions in the IQT™ and those under which the coefficients were derived. For this reason it is important to understand how the conditions experienced by the fuel in the IQT™ differ from those used in the literature and detailed chemical kinetic modelling.

3.3 Understanding Autoignition Behaviour in the IQT™

Unlike shock tubes and rapid compression machines, which are used as sources of autoignition data, the IQT™ is heterogeneous. This is an inherent feature of the IQT™ as fuel is injected into charge air, experiencing continuous changes in fuel/air ratio and possibly ambient conditions (temperature and pressure). In this way the IQT™ is similar to a diesel engine, enabling the good relationship achieved by Yates et al. (2004) between autoignition delay results in the IQT™, and cetane number in the D613.

It is, however, desirable to somehow account for this heterogeneity when attempting to predict the autoignition delay behaviour of fuel sprays. This enables the prediction of autoignition delay based solely on the intrinsic chemical behaviour of the fuel. A widely used method is the coupling of a Computational Fluid Dynamic (CFD) model, to cater for fuel mixing, heating and transport, with a numerical combustion model, to calculate reaction rates and combustion behaviour.

CFD-Detailed chemical Kinetic modelling of autoignition

- In a paper entitled *Numerical Modelling of Autoignition, Combustion, and Soot Formation for n-Heptane Sprays in a High Pressure Constant-Volume Chamber*, Tao et al. (1999) used chemical kinetic modelling in conjunction with a CFD package to model n-heptane combustion and soot emissions in a constant volume combustion bomb at 50 bar and 800 K. The SENKIN[ii] code in CHEMKIN was used to model the chemical reactions with a reduced reaction size of 57 species and 212 reactions. The KIVA3 CFD package was used to model spray atomisation, collisions, evaporation and transport, with the k-ε turbulence model for the simulation of turbulence. The reduced chemical model was calibrated against literature data to ensure that it still showed the characteristic high temperature, low temperature and negative temperature (NTC) behaviour of n-heptane.

  The modelled autoignition delays and soot formation were found to be in good qualitative agreement with shock tube data from the literature. Importantly, the

[ii] A module of CHEMKIN; a commercial code used for detailed chemical kinetic modelling.

model was able to report NTC behaviour in the 600-900K temperature range, which is essential for accurate autoignition modelling of fuel sprays.

- The same approach was used by Tao et al. (2000) in another paper entitled *Self-Ignition and Early Combustion Process of n-Heptane Sprays Under Diluted Air Conditions: Numerical Studies Based on Detailed Chemistry*. Again the study involved modelling of n-heptane injection and combustion in a high temperature, high pressure, constant volume combustion bomb. The goal was to accurately determine autoignition delay, investigate flame lift-off and to evaluate the effects of charge air dilution on autoignition delay.

  Detailed chemical kinetics, with reduced mechanisms (65 species and 273 reactions), was used to model the combustions of the fuel while KIVA3V CFD code was used to model the spray behaviour via an Arbitrary-Lagrangian-Eulerian (ALE) approach. A sub-grid Partially Stirred Reactor (PaSR) model was used to account for turbulence-chemistry-interactions, and the RNG k-ε model was used to simulate turbulence in the combustion chamber.

  An argument is made for the use of detailed chemical kinetic modelling for the correct modelling of combustion. The authors argue that simpler models, such as single stage reaction models or the Shell autoignition model (a much reduced reaction mechanism consisting of 5 reactions and 8 species), are inadequate to describe the post ignition behaviour and combustion. Furthermore, it is argued that simple models are unable to accurately cater for the effects of gas composition on the autoignition delay behaviour, making it impossible to determine the effects of charge air dilution or EGR.

  To evaluate the impact of the reductions made in their chemical mechanism on accuracy, calculated autoignition delays were compared to shock tube data and showed generally good agreement.

  Experimental data on spray penetration was used to calibrate the grid size for the CFD simulation. It was found that while coarse grid sizes tended to result in an under-prediction of spray penetration, too much grid refinement resulted in an over-prediction. Ultimately it was found that a grid spacing of 1.2mm produced good agreement with the experimental data.

The point of autoignition was defined as the time after which a predefined temperature rise was observed. The literature was consulted for the magnitude of the temperature rise and while the Franz-Kamenetzki theory yielded a number of 30K, previous homogeneous ignition studies were found to use 200K as the criterion. Ultimately a temperature rise of 100K was used as this produced the best agreement with experimental autoignition delay times when using the above mentioned grid size.

Having validated and refined the model the study went on to investigate high-speed injection rates and flame lift-off, which is representative of real diesel injections. The study also investigated the effects of charge air dilution on autoignition delay. Both investigations produced results that were in good qualitative agreement with experimental data.

- A third paper published by Tao et al. (2002) (*Numerical Investigation of Reaction Zone Structure and Flame Lift off of DI Diesel Sprays with Complex Chemistry)*, using this modelling technique was aimed at the simulation of direct diesel injection. The simulations were not of a diesel engine specifically, but rather of a constant volume bomb at engine-type conditions. The main concern of the study was post ignition combustion development and emission formation.

  The model consists of a reduced detailed chemical kinetic treatment (65 species and 268 reactions) for the combustion of n-heptane and a CFD model for the simulation of spray injection, transport and turbulence. Several methods of handling turbulence-chemistry interaction were discussed and compared. The shortcomings of probability density function (PDF) and flamelet techniques were highlighted and it was decided that the Chalmers developed partially stirred reactor (PaSR) model should be used.

  The onset of autoignition, and hence combustion, was defined by a 100K temperature rise, this being consistent with previous work carried out by the authors. It was found that combustion began in a lean area outside of the main spray core, at some distance from the injection nozzle. The combustion then proceeded to move in towards the spray core, crossing the mean stoichiometric region and entering a richer zone. The flame then surrounds the head of the spray and reaches equilibrium such that the flame remains stationary, around the head of the spray and some distance from the injection nozzle.

Although the autoignition point is in the lean zone around the spray core for the above stated definition of autoignition (100K rise in temperature), it was noted that this rise in temperature could be associated with the cool flame reactions which are known to precede the main ignition event. If a larger temperature rise were chosen to indicate autoignition then the point of autoignition could in fact be closer to the spray axis and hence in a richer region.

The study resulted in a well developed understanding of the combustion of an n-heptane spray. The results were in good agreement with a previous theoretical model proposed by Dec (1997), and were able to describe the flame propagation and stabilization as well as the regions of emission formation.

Drawbacks of CFD-Detailed Chemical Kinetic modelling

While it has been shown in studies such as those presented above that the coupling of CFD with detailed chemical kinetic modelling can produce useful results, there are significant drawbacks to the method. These are in the form of computational time and resource requirements. Ali et al. (2003) carried out a study in an attempt to improve the efficiency of this method.

It was found that by systematically reducing the number of chemical mechanisms (as in the work of Tao et al., 1999, 2000, 2002) and using parallel processing, they were able to bring computational time down significantly, while still maintaining good agreement with more detailed chemical mechanisms.

Although the study yielded useful reductions in computational time, the approach involves significant reductions in chemical mechanisms and significant hardware costs. The chemical mechanism for n-heptane was reduced to 25 species and 21 reactions steps to reduce computational time by a factor of 1.76 over an already reduced mechanism of 40 species and 165 reactions. Although the 25 species model showed good qualitative agreement with detailed models it showed significant divergence at some operating points.

The parallel processing produced significantly better reductions in computational time but required multiple processors, making parallel processing an expensive option if significant reductions are desired.

CFD-Arrhenius modelling of autoignition

A much simpler and less computationally intensive method of modelling heterogeneous autoignition was investigated by Cox (2006). This method made use of the empirical formulation proposed by Yates et al. (2004) to predict autoignition delay, in conjunction with the FLUENT® CFD package for the modelling of fuel evaporation, heating and transport.

The study focused on a simplified model of autoignition in the ASTM D613 CFR engine. It consisted of the evaporation of a single drop of fuel under quiescent conditions approximately equal to the conditions in the combustion chamber of the ASTM D613 CFR engine at the start of fuel injection.

This study was important in establishing the method whereby the autoignition delay model proposed by Yates et al., could be coupled to the FLUENT® CFD package. This was achieve by writing a user defined function (UDF) to define a scalar quantity equal to the instantaneous reaction rate in each cell. The scalar quantity was then integrated and added to the already accumulated value of the user defined scalar (UDS). This UDS is the reaction rate integral as defined by Livengood and Wu (1955) which, when equal to unity, indicates the onset of autoignition.

Good agreement was achieved between the modelled autoignition delay and ASTM D613 autoignition data, indicating that this approach could perhaps be used for more complex problems such as fuel injection and autoignition modelling in the IQT™.

3.4 Injection Modelling with CFD

As stated previously, diesel-type combustion is heterogeneous. This precludes the use of global models of autoignition - including detailed chemical kinetic models and empirical models such as that proposed by Yates et al. (2004) - without some knowledge of the changing conditions experienced by the fuel over time. It is essential to understand for example, how the fuel mixes with the surrounding air or what heat transfer takes place to or from the fuel. For this reason it is important that a spray model to be used to aid in the prediction of autoignition be setup with care.

A parametric study by Barroso et al. (2003), dealing specifically with diesel spray simulation, was consulted when setting up the spray model for this study. The study was an investigation of the sensitivity of injection results to various modelling parameters. Of particular interest for combustion bomb modelling, was the sensitivity of the injection to spatial and temporal resolution.

The study was performed by varying the various modelling parameters and comparing the results to experimental data. The experimental data consisted of shadowgraph images for penetration depth analysis and Phase Doppler Anemometry (PDA) for the determination of droplet velocities and diameters. The standard k-ε model was used to model turbulence, the StarCD CFD package was used for droplet transport and reactions and the fuel used was n-dodecane.

The study found that spray penetration depth is very sensitive to the resolution of the mesh of computational cells. An overly coarse mesh leads to an overestimation of the velocity difference between the continuous and discrete phases, resulting in higher drag forces and lower penetration. The opposite is true of too fine a mesh resolution, where the underestimation of the velocity difference between phases leads to overly large penetration depths. It was found that a cell length of 1mm produced penetration depths with a good empirical fit to the experimental results and that, while altering the radial and azimuthal refinement affected the penetration, further axial refinement had little or no effect.

For a constant volume bomb the values of k and ε were initialised to zero as no turbulence was expected at the start of injection. Under these conditions a time step size of 1μs was found to produce good agreement with experimental data.

3.5 Modelling with the FLUENT® CFD Package

The FLUENT® manuals for general use and User Defined Functions were used extensively throughout the project. The former was consulted when setting appropriate values for the various user inputs, while the latter contains the detailed information necessary for writing UDFs in FLUENT®, such as the types of UDFs available and the necessary steps needed to properly implement them.

4 Modelling Methodology

It was decided that in order to gain an understanding of the autoignition delay behaviour of fuels in the IQT™, a CFD model would be developed. The model would consist of an injection model, to account for spatial and temporal variations in the conditions experienced by the fuel, and an implementation of the Yates model, as proposed by Cox (2006), to indicate the initiation of autoignition. A more detailed description of the modelling philosophy is presented below.

Modelling the IQT™ Combustion Chamber and Injection

The IQT™ was modelled using the FLUENT® CFD package. The initial pressure and temperature values were based on measurements taken inside the IQT™ at various test temperatures. This allowed a more detailed initialisation of the temperature profile than simply using the test temperature reported by the IQT™, at a single point in the combustion chamber. The use of a temperature profile, as opposed to a single homogeneous temperature, was considered important because of the suspected influence of a temperature history on ignition delay in the IQT™.

FLUENT® has a built-in utility for creating injections, and this was used to simulate injection into an axisymmetric two-dimensional representation of the IQT™ combustion chamber.

Autoignition modelling

A recent addition to the FLUENT® package is a built-in utility for determining ignition delays based on the model presented by Douaud and Eyzat. (1987). This standard package model is based on a single Arrhenius equation and it does not allow for the possibility of negative temperature coefficient behaviour in the intermediate temperature zone which is relevant and pertinent to the IQT operating regime (Yates et al., 2004). Furthermore it was an explicit intention of this investigation to validate the model developed by Yates et al as a convenient descriptor of the intrinsic ignition delay behaviour of n-heptane. For these reasons the user defined function (UDF), developed by Cox (2006) to implement the original Yates model as described in Equation 2-14, was modified and implement to perform the improved Yates model shown in Equation 2-16.

Fuel History Tracking

Finally, in order for the model to produce a useful output, it was necessary to extract a record of the changing conditions experienced by the fuel responsible for initiating autoignition. For this purpose an inert particle was injected into the fuel stream and allowed to be swept along by the flow field in the combustion chamber. A second UDF was incorporated into the model to write an Excel® compatible output file containing the temperature, pressure, position and fuel/air equivalence ratio in the region of the inert particle at each computational time step. This representative trajectory could be used to describe the conditions experienced by a fuel molecule - that initiates autoignition - in the IQT™ as a function of time. This enables the use of measured ignition delay in the IQT™ as data for the characterisation of the chemical autoignition behaviour of fuels.

Now that the modelling philosophy has been broadly covered, a more detailed description of the modelling procedure can be covered with some basic frame of reference. The modelling task involved in this investigation can be divided into four main parts:

- Pre-initialisation model setup
- Appropriate application of initial conditions
- Application of the Yates model for autoignition prediction
- Recording of the fuel trajectory

For clarity each of these will be dealt with individually.

4.1 Pre-initialisation Model Setup

Solver selection

The problem never reaches steady-state and therefore it requires an unsteady formulation. The segregated, implicit solver was selected for its efficient use of resources. In the interest of reducing computational time it was decided that an axisymmetric model would be used. FLUENT® offers two ways to deal with axisymmetric space; one with axisymmetric swirl and one without. Due to the high

level of symmetry about the axis in the IQT™ there was no reason to believe that any significant swirl would develop. For this reason axisymmetric swirl was not enabled.

A one microsecond time step size was selected as this resulted in the best compromise between time-to-solution and stability. This was also shown by Barroso et al. (2003) to be an effective time increment for the grid size indicated below.

Computational mesh

The layout of the modelled domain is shown in Figure 4-1, with all of the relevant features labelled.

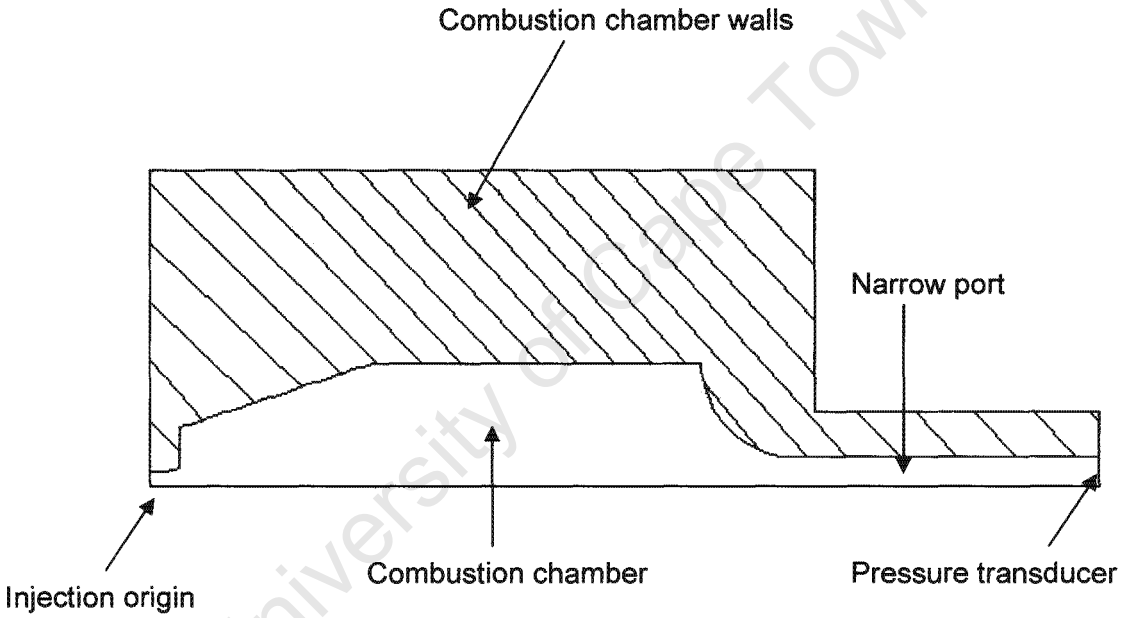

Figure 4-1. Layout of the IQT™ geometry.

The computational mesh comprised 1mm axial spacing and varying radial spacing, where axial refers to the axis of the IQT™ and of the spray. This was found to be stable and to predict realistic spray structure and penetration. Barroso et al. (2003) showed that while further axial refinement had little effect on modelled spray penetration, appropriate radial refinement is important to properly resolve the velocity difference between the discrete and continuous phases. It is this velocity profile that is responsible for the drag on the particles and hence the ultimate penetration behaviour.

It is also important to realise that excessive refinement in the axial direction leads to an increasingly small time step requirements as it is desirable to have a time step smaller than that time taken for a particle to traverse a cell

For this reason, further refinement was carried out in the radial direction only, with cell sizes increasing from 0.5mm near the spray axis to 1mm near the combustion chamber walls, resulting in the mesh seen in Figure 4-2.

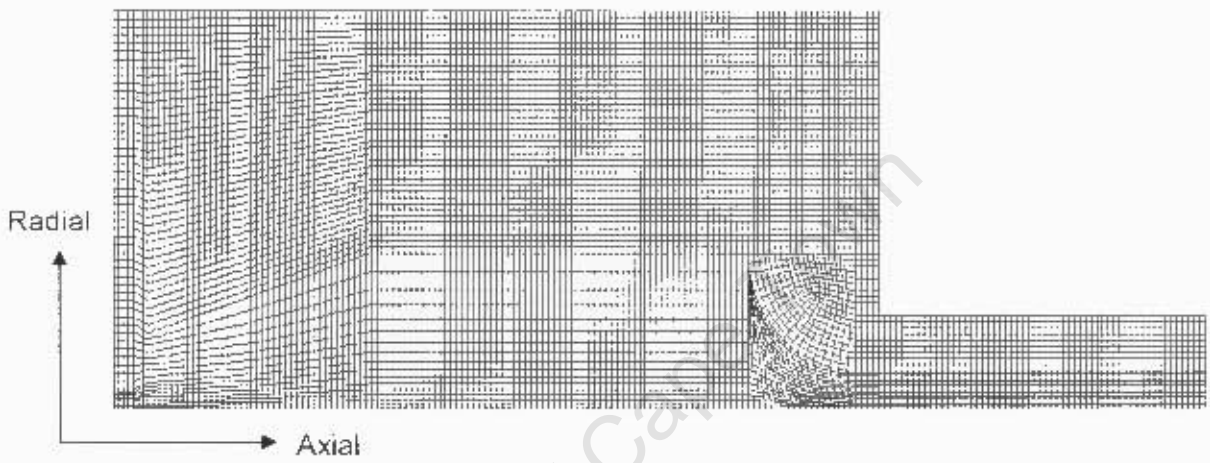

Figure 4-2. 2D Axisymmetric mesh of the IQT™ combustion chamber and walls.

Turbulence modelling

The Renormalization Group (RNG) version of the k-ε model was used to model turbulence in the combustion chamber. The standard k-ε model has, like its RNG derivative, been used extensively to successfully model injection (Ahmadi-Befrui et al., 1991; Tao et al., 1999; Tao et al., 2000; Tao et al., 2002; Ali et al., 2003; Barroso et al., 2003; Gustavsson et al., 2004), however the RNG version, while similar to the standard model, proved to be more stable in this application.

Fuel Injection setup

The n-heptane injection was modelled using the discrete phase transport and injection model provided in FLUENT®. This allows the simulation of a discrete phase in a Lagrangian frame of reference, with an Eulerian treatment for the continuous phase. The n-heptane particles were two-way coupled to the continuous phase thus generating turbulence and air entrainment, whilst also being slowed and dispersed. Based on the injection duration and the required mass of fuel per injection (0.098

grams of hexadecane (Advanced Engines Technology, 2003) and therefore approximately 0.087 grams of n-heptane), the average flow rate of the fuel could be calculated. The injector specifications (International Organisation for Standardization (ISO), 1998) allowed an approximation of the area through which the fuel flows. Given the flow rate and nozzle area it was determined that the initial velocity of the fuel would be approximately 209 m/s.

Four point- injections were used to generate the spray pattern shown in Figure 4-3. They were equally spaced along the injection face creating the radius of the injector nozzle. Each point-injection was assigned a direction vector in order to simulate a solid, narrow-cone injection structure. FLUENT® includes a solid cone injection as a standard injection type unfortunately this is only available for three-dimensional modelling.

The injection temperature was set at a temperature slightly lower than the temperature measured on the face of the injector in the combustion chamber. This was done because some heat loss would occur from the fuel to the cooling water surrounding the injector. The same temperature (480K) was used regardless of the test temperature being modelled. This was seen as reasonable as the flow rate of the injector coolant is varied to maintain a constant nozzle temperature, thereby removing more or less heat from the fuel.

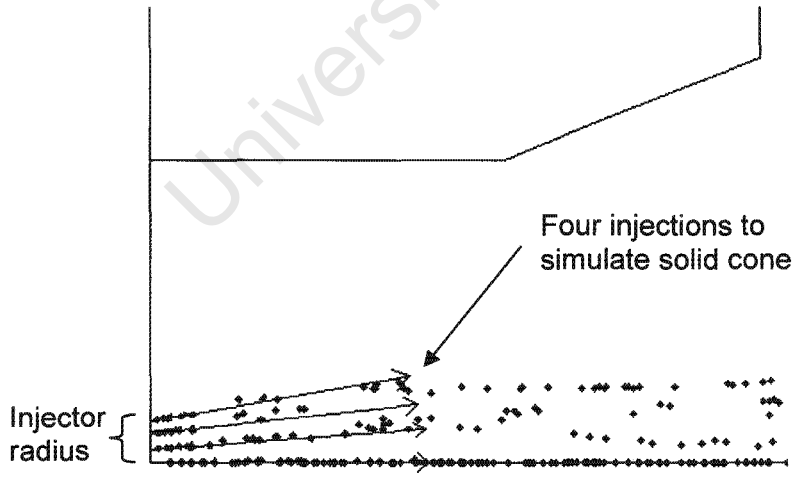

Figure 4-3. Injection origin showing four injection streams.

The isobaric material properties of n-heptane for a range of temperatures were obtained from the NIST WebBook[iii]. This data was used to provide a piecewise-linear

[iii] Online, available: http://webbook.nist.gov/cgi/fluid.cgi?ID=C142825&Action=Page

description of the properties of n-heptane for the temperature range of interest. The boiling point and mean value of the latent heat of vaporisation were calculated for the same temperature range using the formulations given by Rose et al. (1977).

4.2 Initial Conditions

Temperature initialization

The physical layout of the IQT™ is such that it is heated along the centre section of its axis by an array of circumferentially spaced cartridge heaters. The injector is located at one end of its axis while a pressure transducer is located at the other end. The injector is cooled and maintained at a nominal temperature of 50°C. The pressure transducer is also cooled and under standard operating conditions is maintained at a nominal temperature of 130°C.

With heating in the middle and cooling on either end it is inevitable that a temperature gradient will exist along the axis of the IQT™. In order to establish the shape of the temperature profile it was measured using a thermocouple. The thermocouple was inserted axially in place of the injector and its depth was varied in 10mm increments to establish the temperature as a function of position along the axis.

To eliminate the effects of conduction along the length of the thermocouple, the temperature near the injector was measured again, this time with the thermocouple inserted from the pressure transducer end. The combined axial measurements were then verified with radial measurements taken at two discrete axial locations. This procedure was carried out at various test temperatures and a typical temperature profile is shown in Figure 4-4.

The profile in Figure 4-4 was approximated by two quadratic equations. The first of these describes the temperature as a function of axial penetration from zero (at the injection origin) to 25 mm. The second describes the remainder of the profile. By dividing the computational domain into two parts, these equations could be applied to describe the initial temperature field as a function of grid position.

No radial variation was included as the radial temperature profile could only be measured at two points along the IQT™ axis. Furthermore the radial profile was very homogeneous, and while a slight increase in temperature was observed (~5 K) near

the walls, it would have required an unjustifiable increase in the complexity to implement.

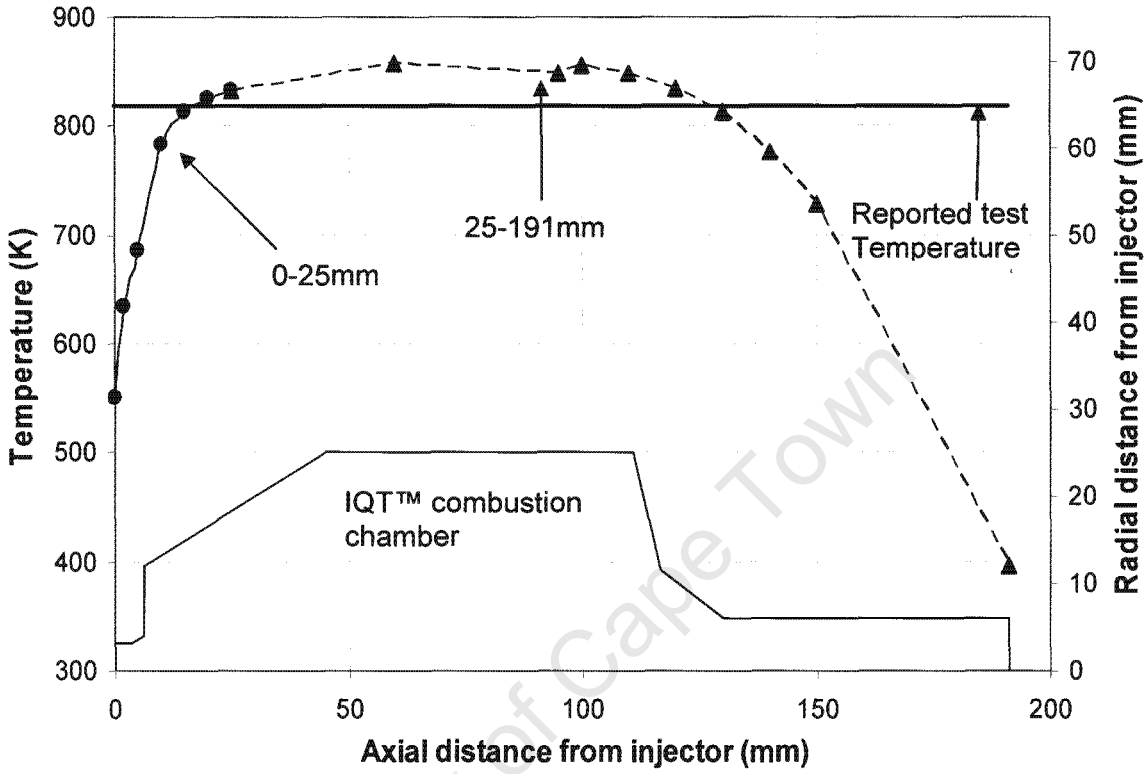

Figure 4-4. Typical measure temperature profile in the IQT™ (profile shown at the standard IQT™ test temperature).

Turbulence initialization

When it is operating normally, the IQT™ performs a series of injection tests for which data is reported. The time between each test is roughly 15 seconds and this interval allows for the heating and settling of the fresh charge air. For the initialization of turbulence the values of k and ε were both set to zero. This was regarded as a reasonable assumption as the time between each IQT™ measurement is relatively long.

4.3 Autoignition Prediction

Integration of the reaction rate

Equation 2-16 is an empirical formulation for the ignition delay, the inverse of which is the reaction rate. Livengood and Wu (1955) defined the point of autoignition as the time at which the integral of the reaction rate with respect to time reaches a value of unity. If the temperature, pressure and air/fuel ratio were constant with respect to time then the point of autoignition would simply be equal to the ignition delay, as defined by Equation 2-16. However if these parameters vary over time, as is the case in the IQT™, then an accumulative approach must be taken. In this way autoignition would be achieved when:

$$\sum_{t=0}^{t=t_{AI}} \frac{\Delta t}{\tau} = 1 \qquad \text{(Eq 4-1)}$$

Where Δt is an incremental change in time, τ is the instantaneous reaction rate given by Equation 2-16 and t_{AI} is the time at which autoignition occurs.

Implementation in the CFD model

It is possible to prescribe user defined scalar (UDS) quantities in FLUENT® by using a specific User Defined Function (UDF). Individual values of the UDS are calculated on a cell-by-cell basis and, once defined, are returned to the solver as source terms for each cell. In this way it is possible to calculate the instantaneous reaction rate in every cell, at any time step and assign the value to the UDS in the cell. Once returned to the solver as a source term, the UDS is integrated with respect to time along with all other solver variables.

The UDS is cumulative and subject to mass flux so that the value in each cell will increase due to the incremental addition of the source term at every time step, as well as due to the contribution from flow into the cell from neighbouring cells. The onset of autoignition is assumed to be indicated by the value of the reaction rate integral (cumulative value of the UDS) reaching unity in any cell.

The A, n, B, C and m coefficients used in the Yates model (Equations 2-16 to 2-19) are listed in Appendix 2. For the purposes of the current work a value of 1.35 was

used for γ in Equations 2-17 and 2-18. This is essentially equivalent to an assumption of constant pressure behaviour in the IQT™.

4.4 Fuel Trajectory Tracking

Inert particle setup

In order to simulate the history of the fuel it was necessary to create a new injection, consisting of a small, inert tracking particle that would be transported by the flow field in the same way as the material surrounding it, thereby experiencing the same temporal variations in pressure temperature and fuel/air ratio and ultimately ending up near the point of autoignition.

The fuel starts out as liquid droplets with relatively high density; the droplets then evaporate and add to the air/fuel mixture in the chamber. A heavy tracking particle may be swept along in the same way as a droplet but would not mimic the movement of the evaporated gaseous mixture very well. For this reason the density of the tracking particle was constantly varied to match the density of the surrounding computational cell. This allowed the tracking particle to match the behaviour of the material surrounding it with respect to the flow field.

The particle was inert and therefore did not undergo any of the phase change reactions experienced by the fuel. This was however, not necessary, as the inert particle is only used to observe the condition of the fluid surrounding it. As an observation tool the inert particle must move naturally in the fluid flow and be as unobtrusive as possible; not taking part in any reactions or significantly impacting the behaviour of the fluid flow around it.

Recording of the inert particle trajectory

In order to determine the conditions experienced by the fuel moving along roughly the same trajectory as the inert particle, a second UDF was written. This new UDF was performed once at the end of each time step. It worked by identifying the computational cell in which the inert particle was located. Once the cell was identified, the pressure, temperature and fuel/air ratio in that cell was written to file. The file was written in a comma-separated values (csv) format so that the data was easily accessible via Excel®.

5 Results

This section will present the results of the work carried out in this project. The discussion of the results is reserved for the next chapter in order to preserve the clarity of the presentation made here.

The results are presented in the following order:

- Results of the temperature profile measurements in the IQT™.
- Results of the CFD autoignition modelling.
- Results of the inert particle history tracking.

5.1 IQT™ Temperature Profile

Modelled temperature profile

When the CFD modelling first began the IQT™ was not available. For this reason the temperature profile in the IQT™, which was believed to be heterogeneous, could not be measured.

In order to provide some insight into the level of heterogeneity, and to provide an initialization profile for early autoignition modelling, the heating of the IQT™ combustion chamber was modelled. This was done by modelling a representative slice of the IQT™, including one of the nine circumferential heaters, the steel walls and the charge air. The arrangement used is shown in Figure 5-1.

All of the important features are labelled on the image. It is important to understand that the nozzle face and the pressure transducer face were held at constant temperatures. These temperatures were the nominal values specified in the IQT™ manual for the injector nozzle and pressure transducer respectively.

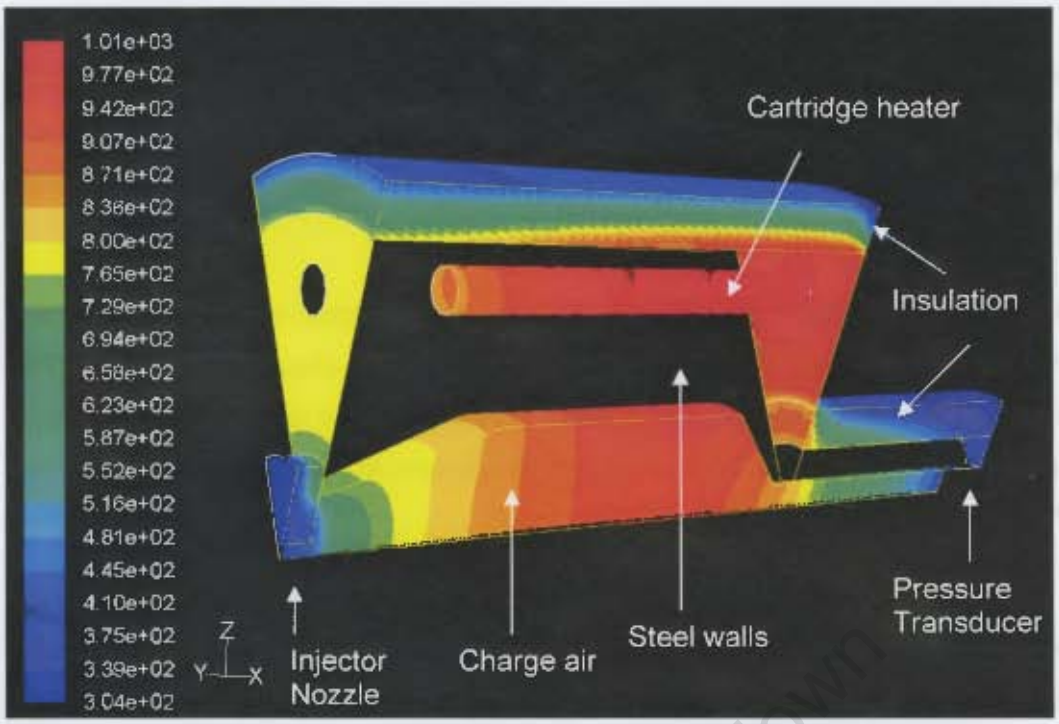

Figure 5-1. Modelling the heating of the IQT™.

Figure 5-2 shows a comparison between the modelled temperature profile, and the profile that was eventually measured, at the standard test temperature, in the IQT™.

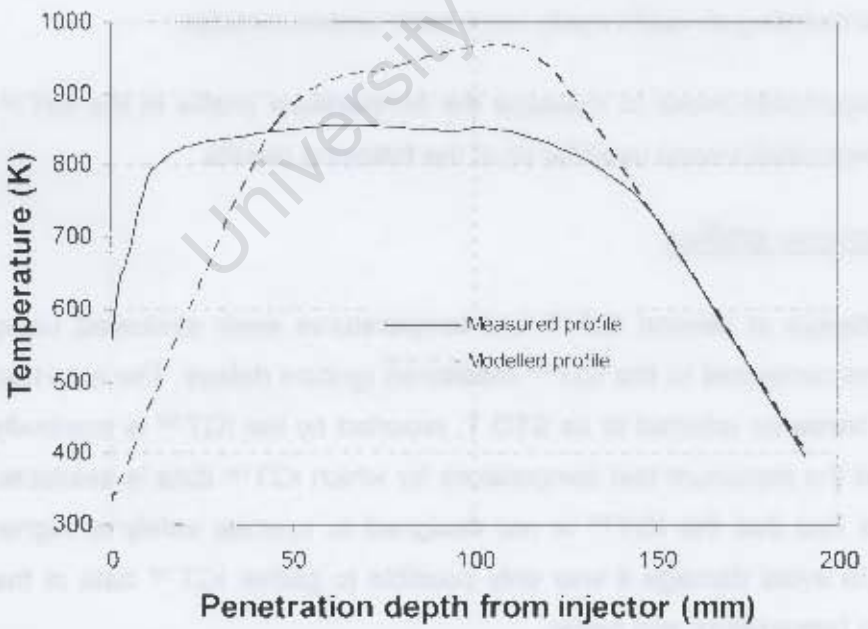

Figure 5-2. Comparison between modelled and measured temperature profiles.

It is clear from Figure 5-2 that there is good qualitative agreement between the modelled and measured temperature profiles. The modelled temperature profile reaffirmed the belief in a heterogeneous temperature profile and motivated the investigation which led to the measured temperature profiles that were ultimately used to model the IQT™.

Figure 5-2 also indicates how important it was to take physical measurements in the IQT™, as the model was unable to accurately predict the shape of the profile. The main discrepancies can be seen in an under prediction of the temperature at shallow penetration depths, and an over prediction of the temperature at the centre of the IQT™.

The reason for the under prediction of the temperatures at shallow penetration depths is due to the fact that the temperature on the nozzle face was maintained at a nominal temperature of 54 °C in the model. In reality this is not the temperature on the face of the injector nozzle inside the IQT™, but rather in the cooling jacket surrounding the injector body.

The over prediction of the temperature at the centre of the IQT™ was most likely caused by an optimistic treatment of the power delivery from the heater and the heat loss to the surroundings. The heater was assumed to be perfectly efficient and the heat loss to the surrounding air could easily have been underestimated.

Fortunately the opportunity arose to measure the temperature profile in the IQT™. The measured temperatures were used for all of the following results.

Measured temperature profiles

The autoignition delays at several IQT™ test temperatures were evaluated using CFD modelling and compared to the IQT™ measured ignition delays. The standard test temperature, hereafter referred to as STD T, reported by the IQT™ is nominally 818K and it is also the maximum test temperature for which IQT™ data is available. This is due to the fact that the IQT™ is not designed to operate safely at higher temperatures, so to avoid damage it was only possible to gather IQT™ data at the standard operating temperature and below.

The bulk of this work is concerned with the operating points for which IQT™ data is available and these points are listed in Table 5-1.

Table 5-1. List of evaluated test points (with IQT™ data)

Test Point	Reported Test Temperature (K)
STD T	818
STD T – 50	768
STD T – 100	718
STD T – 150	668

Although no IQT™ measurement were possible at higher temperatures due to materials limitations, it was nevertheless desirable to use the CFD model to qualitatively forecast the IQT™ autoignition delays for higher temperatures. These high temperature operating points are listed in Table 5-2.

Table 5-2. List of evaluated test points (without IQT™ data)

Test Point	Derived Test Temperature (K)
STD T + 50	868
STD T + 100	918
STD T + 150	968

Figures 5-3 shows the results of the temperature measurements taken at each of the reported test temperatures listed in Table 5-1.

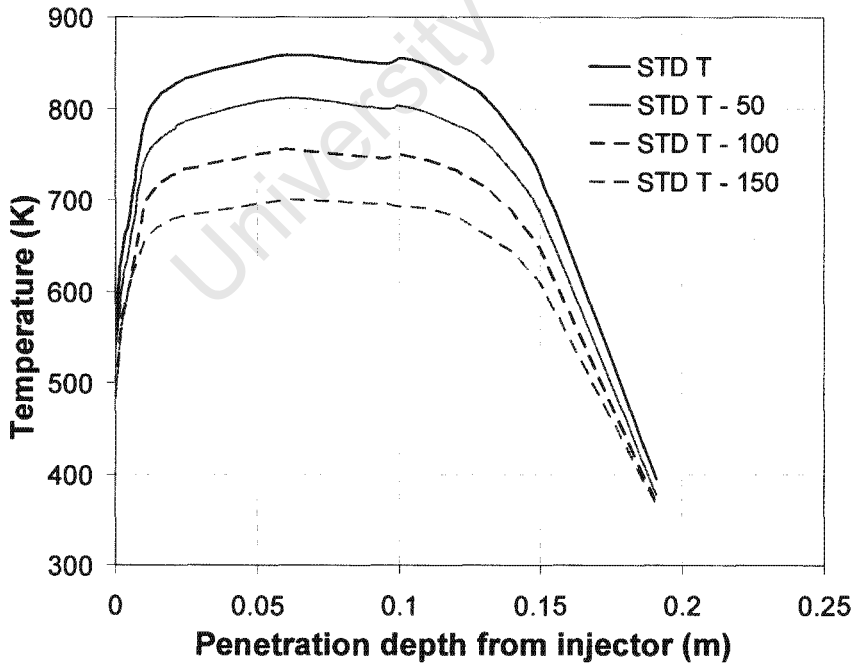

Figure 5-3. Measured, low temperature profiles in the IQT™.

The temperature profiles used for the tests listed in Table 5-2 could not be measured and were therefore derived by linear interpolation based on the measured profiles shown in Figure 5-3. The derived profiles are shown in Figure 5-4.

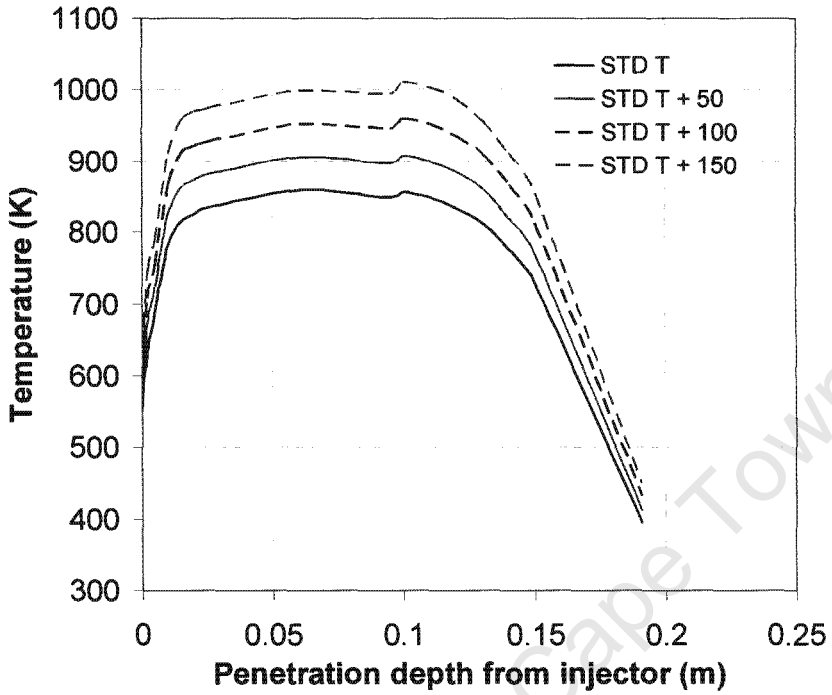

Figure 5-4. Derived, high temperature profiles in the IQT™.

5.2 CFD Autoignition Modelling

With the Yates model of autoignition delay implemented via the UDS it was possible to observe the progress of the reaction rate integral over time along with the position of the point closest to autoignition. This was done using the post processing capabilities of FLUENT® to display flow properties graphically. In the same way it was possible to observe the corresponding changes in temperature and fuel/air ratio.

Example of results visualization

The following example is of the modelling of n-heptane autoignition at 150 °C below the standard test temperature. Figures 5-5 and 5-6 show changes in temperature and fuel/air ratio[iv], respectively. Figure 5-7 shows the corresponding change of the reaction rate integral over time.

[iv] This is not to be confused with the fuel/air *equivalence* ratio normally referred to in this report.

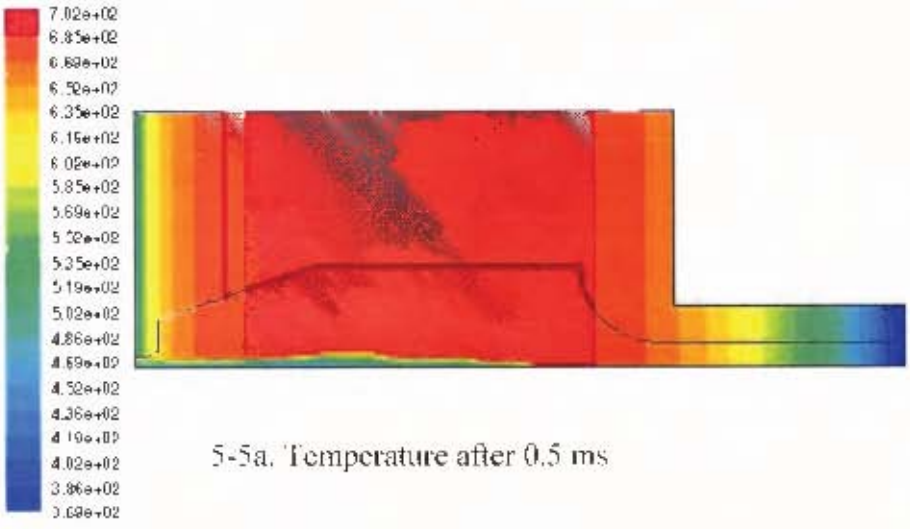

5-5a. Temperature after 0.5 ms

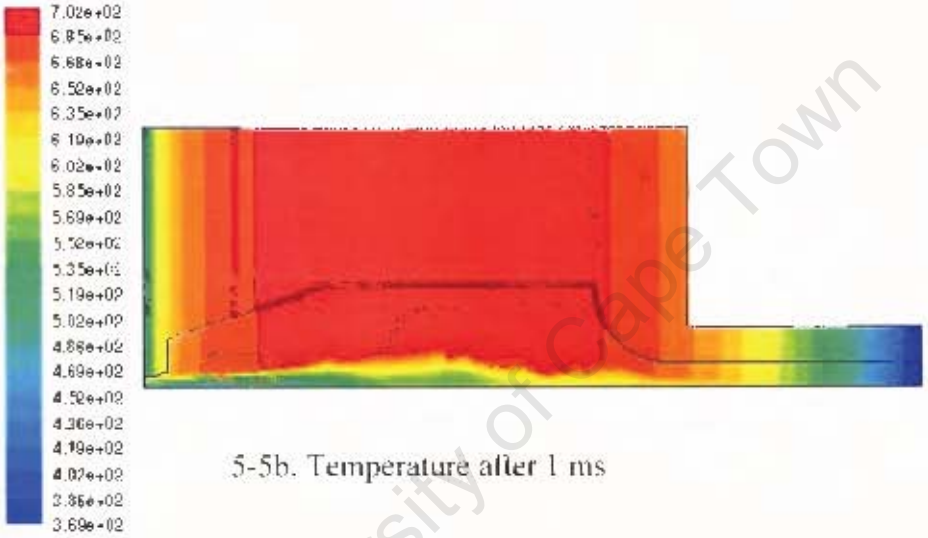

5-5b. Temperature after 1 ms

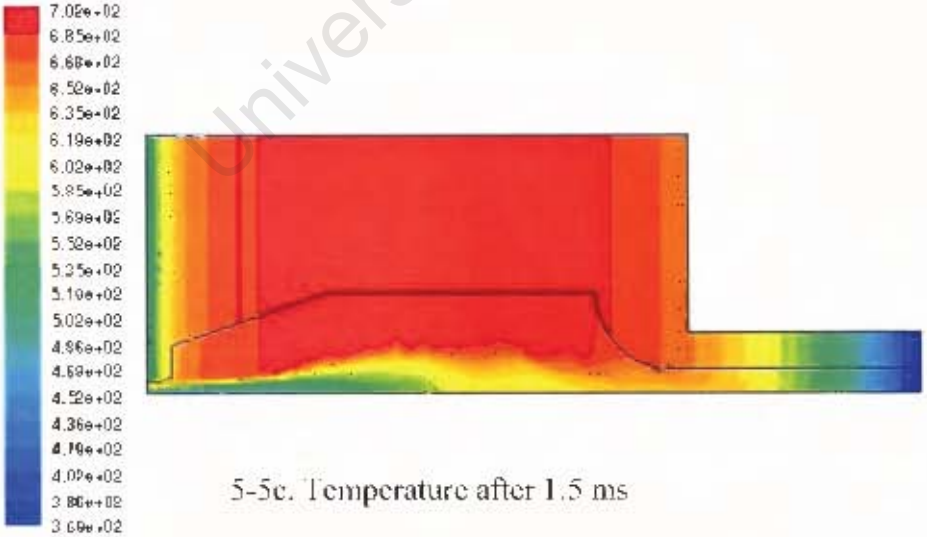

5-5c. Temperature after 1.5 ms

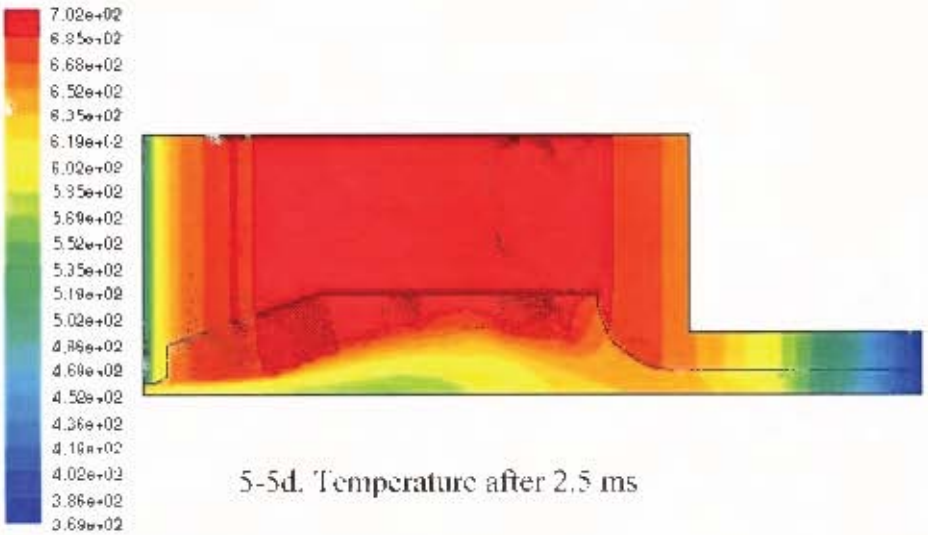

5-5d. Temperature after 2.5 ms

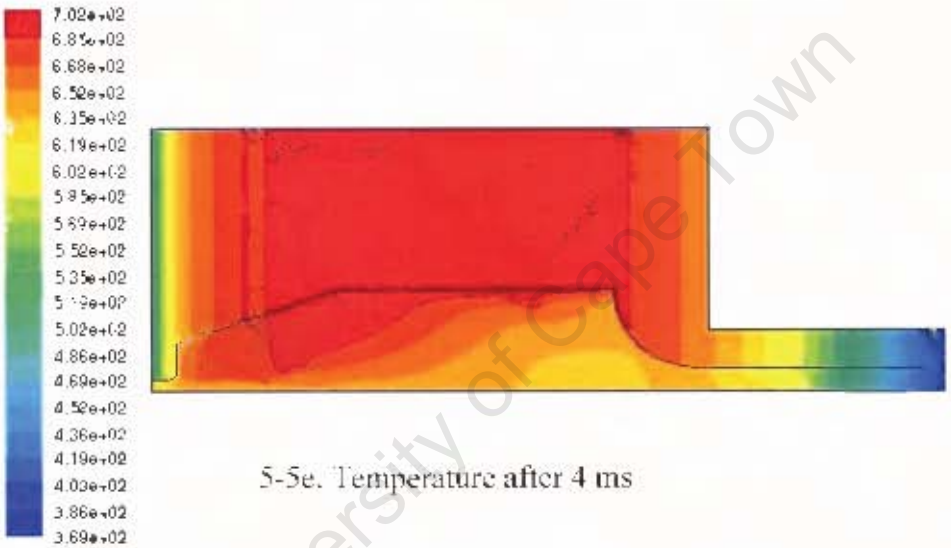

5-5e. Temperature after 4 ms

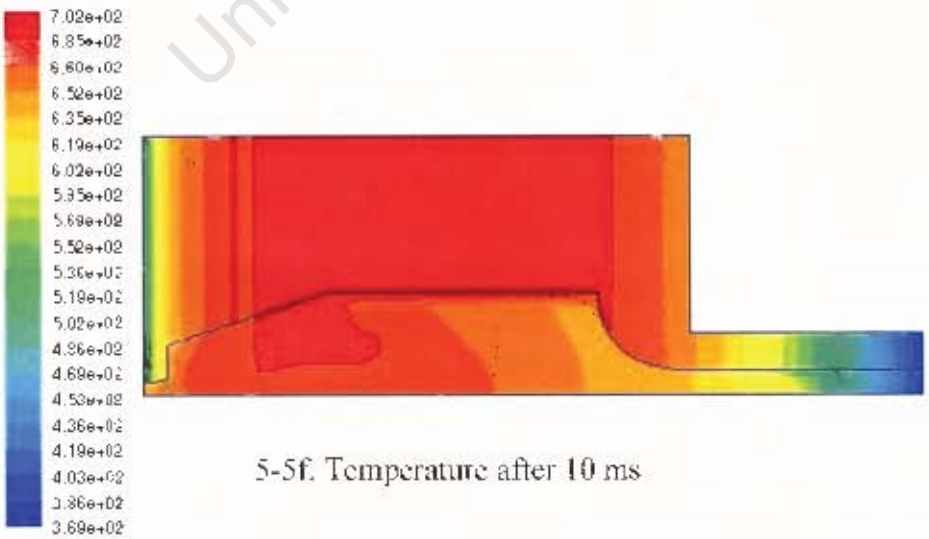

5-5f. Temperature after 10 ms

Figure 5-5. Visualisation of the change in temperature in degrees Kelvin, over time, at STD T – 150.

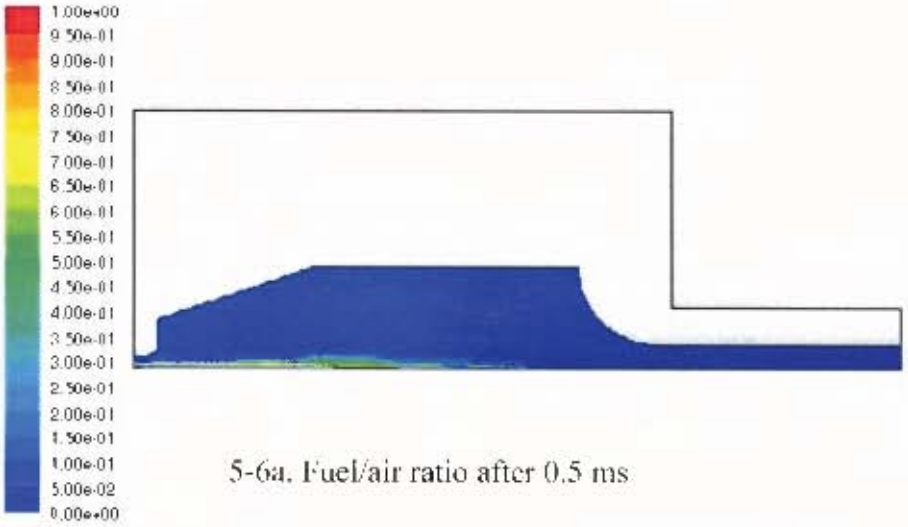

5-6a. Fuel/air ratio after 0.5 ms

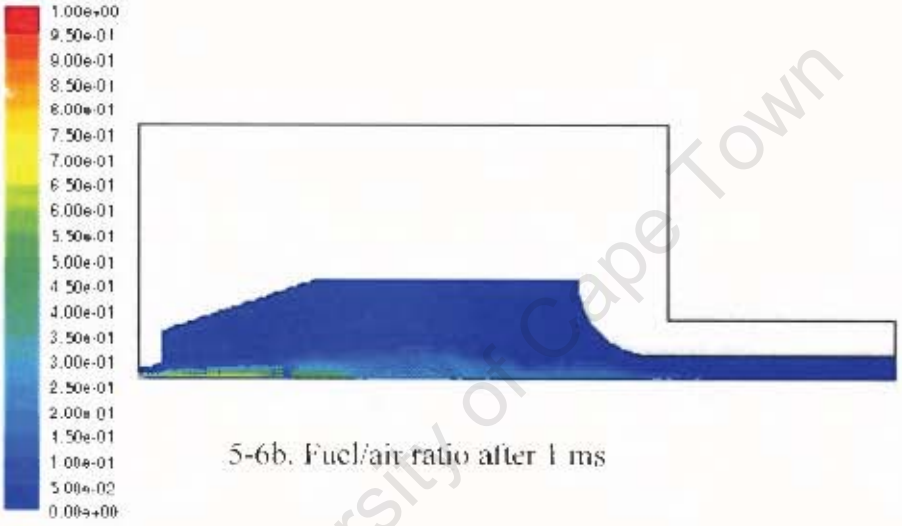

5-6b. Fuel/air ratio after 1 ms

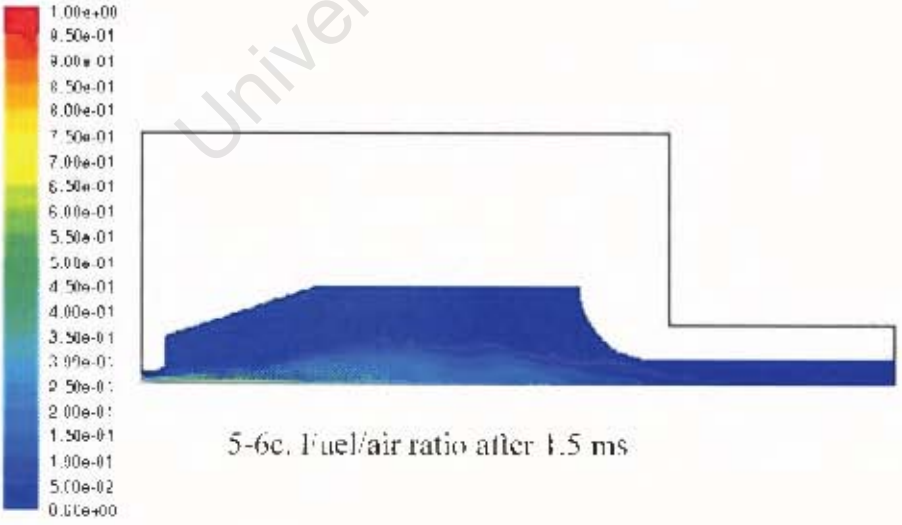

5-6c. Fuel/air ratio after 1.5 ms

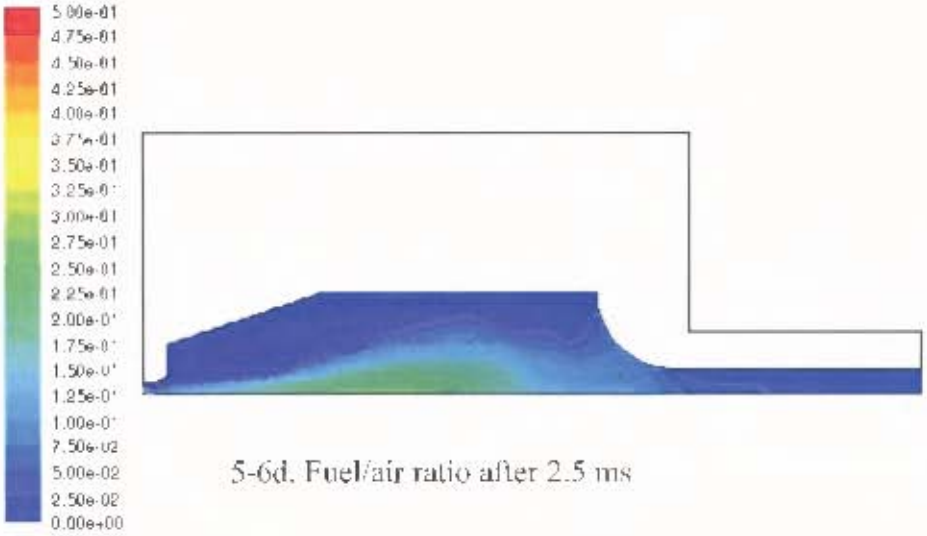

5-6d. Fuel/air ratio after 2.5 ms

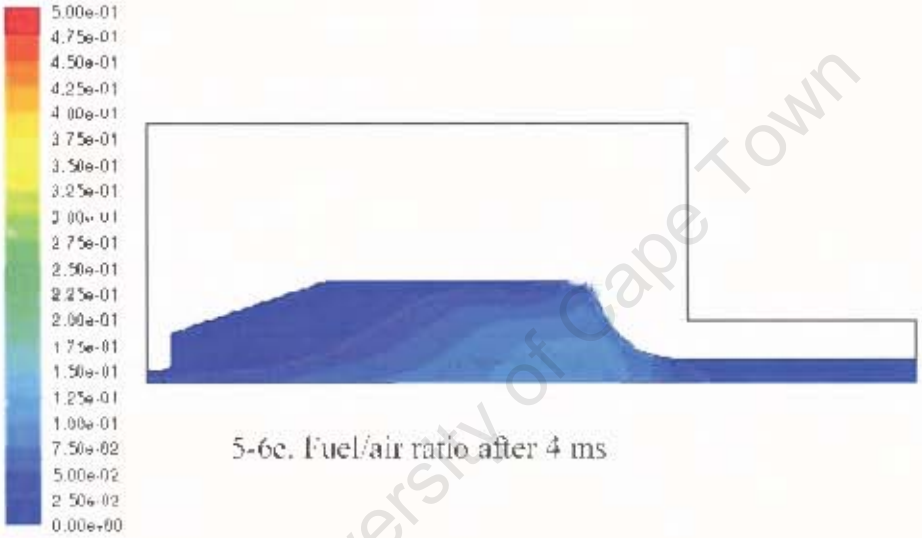

5-6e. Fuel/air ratio after 4 ms

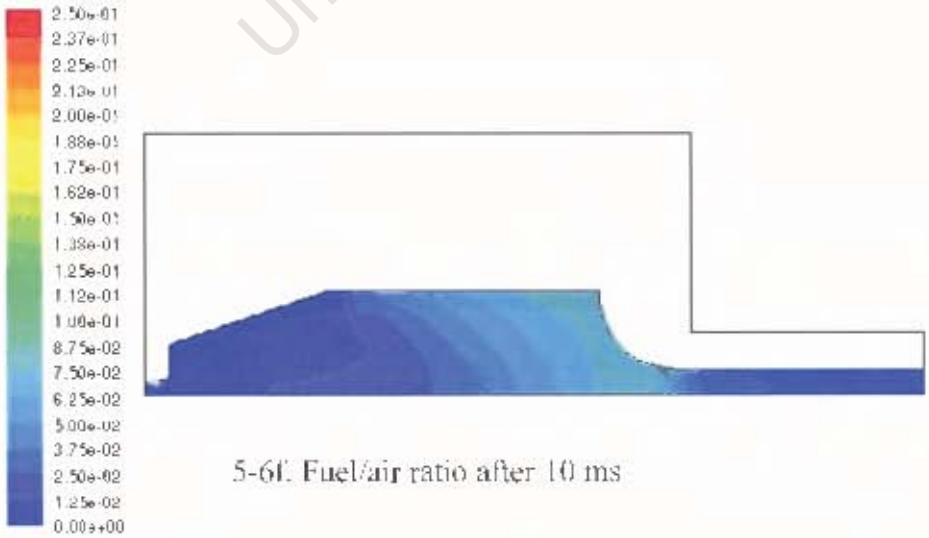

5-6f. Fuel/air ratio after 10 ms

Figure 5-6. Visualisation of the change in fuel/air ratio over time at STD T – 150 (Note: The maximum value in the legend varies).

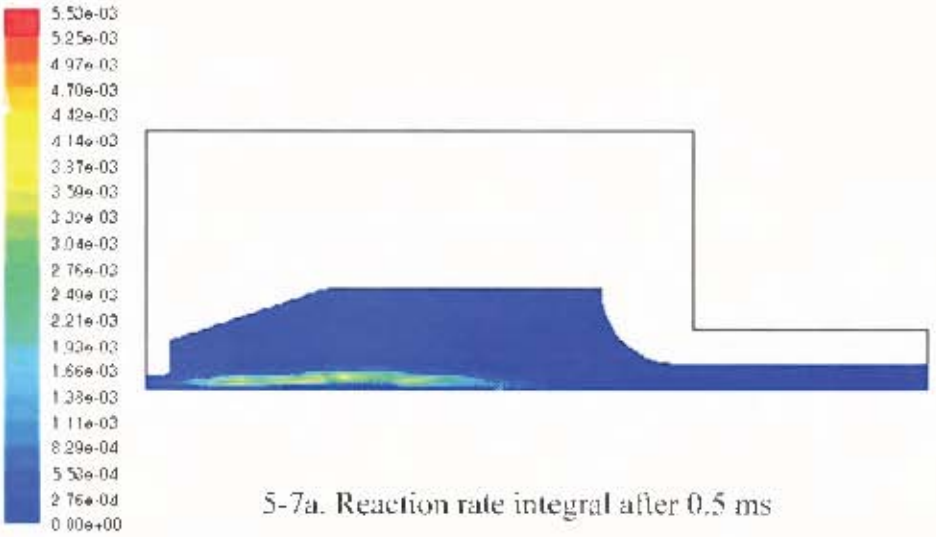

5-7a. Reaction rate integral after 0.5 ms

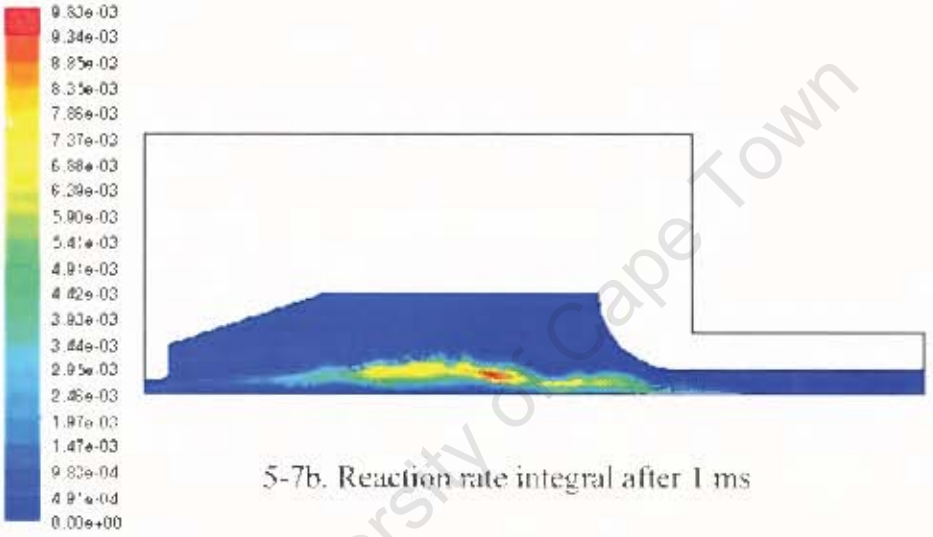

5-7b. Reaction rate integral after 1 ms

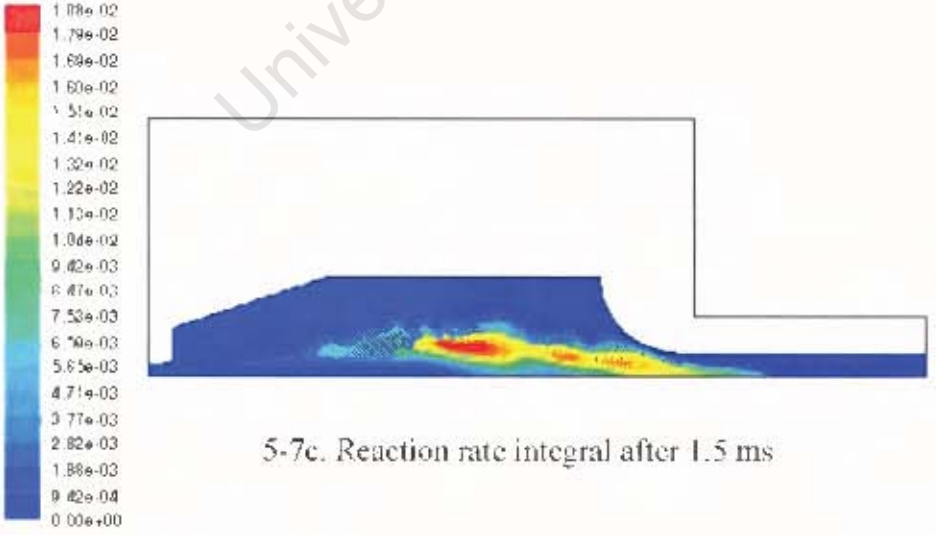

5-7c. Reaction rate integral after 1.5 ms

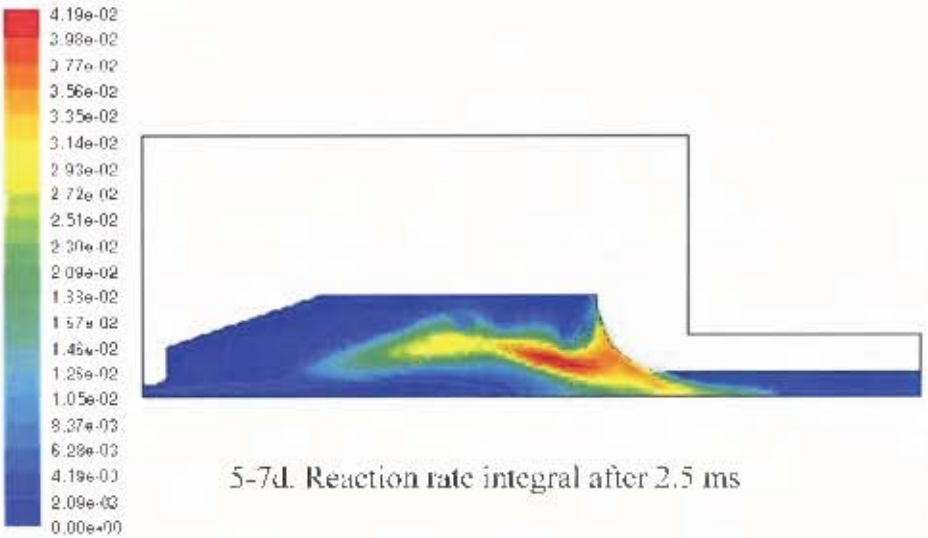

5-7d. Reaction rate integral after 2.5 ms

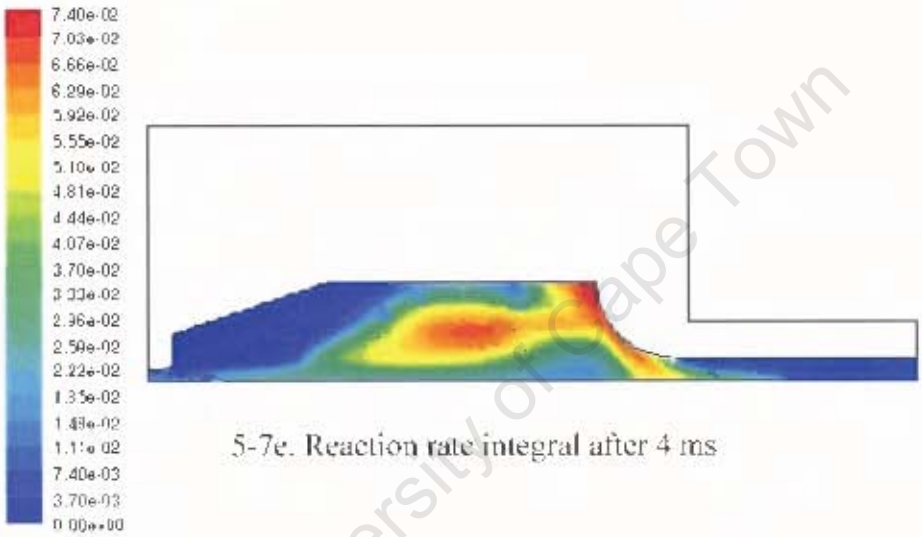

5-7e. Reaction rate integral after 4 ms

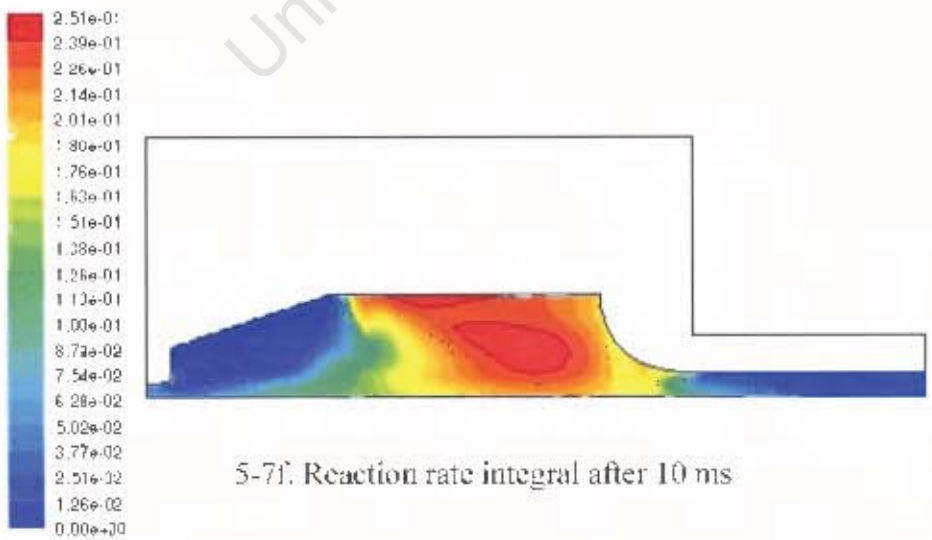

5-7f. Reaction rate integral after 10 ms

Figure 5-7. Visualisation of the progress of the reaction rate integral over time at STD T – 150 (Note: The maximum value in the legend varies).

Effects of changing the test temperature

The point of autoignition was observed to change its position in the combustion chamber with changing test temperature and hence, residence time in the bomb. It occurred at the entrance to the port leading to the pressure transducer for short ignition delays, being guided by the walls and doubling back towards the injector for longer delays.

Figures 5-8 to 5-11 show the autoignition point for each of the test temperatures for n-heptane.

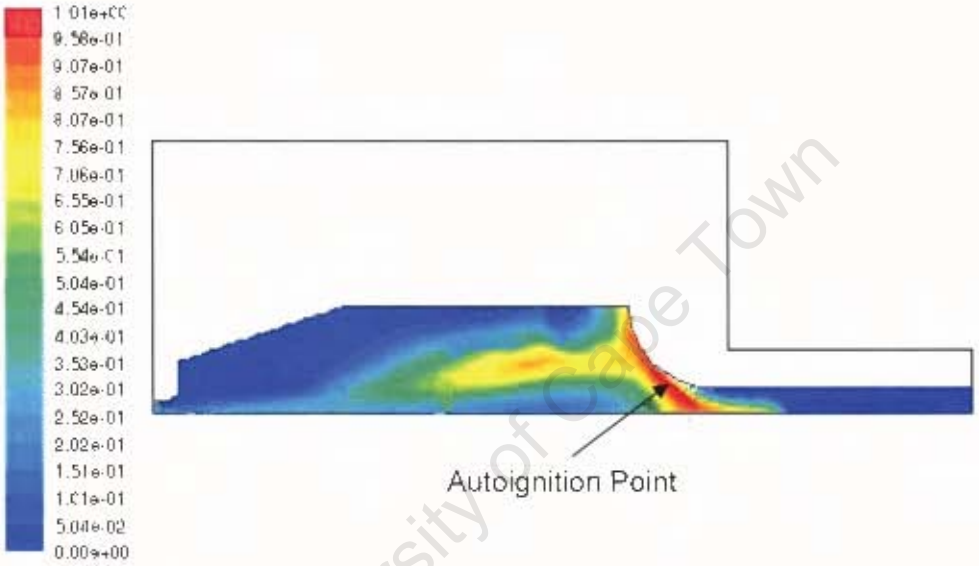

Figure 5-8. Autoignition point at STD T (3.2 ms).

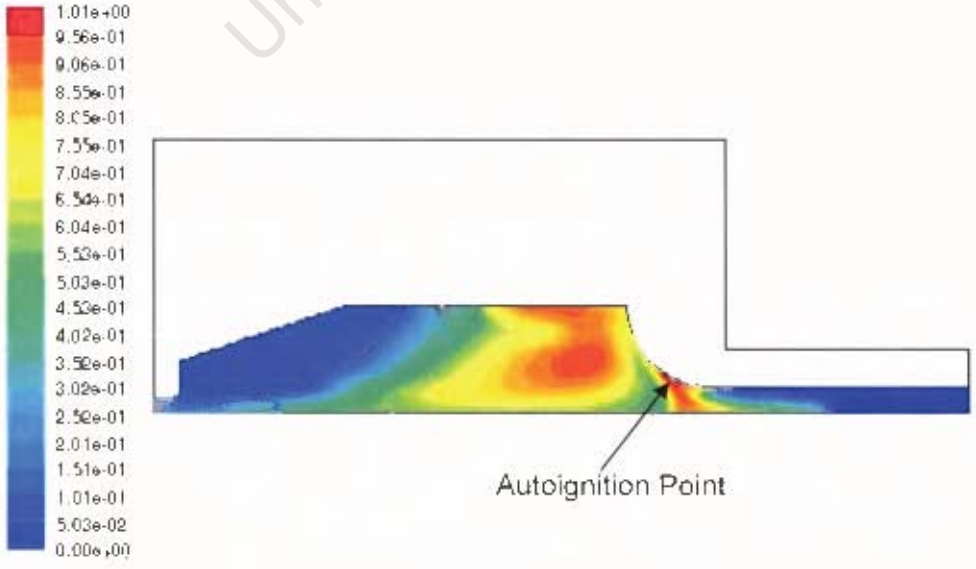

Figure 5-9. Autoignition point at STD T – 50 (5.1 ms).

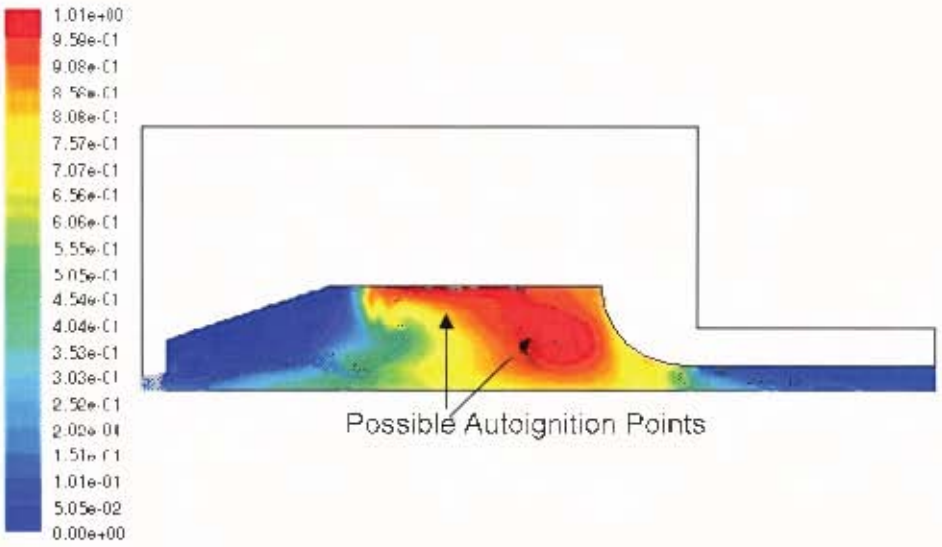

Figure 5-10. Autoignition point at STD T – 100 (10.1 ms).

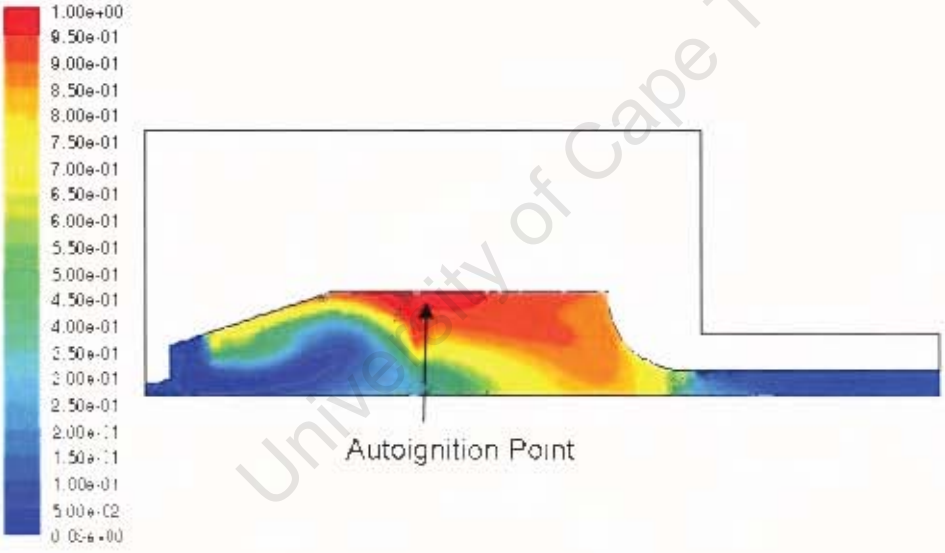

Figure 5-11. Autoignition point at STD T – 150 (29.7 ms).

The fact that the location of the ignition point was variable is a further indication that an assumption of homogeneous values for temperature a fuel/air ratio is inappropriate. The fuel that ignited in the position shown in Figure 5-11 had almost certainly experienced a different history with respect to its test temperature than the fuel that ignited in the position shown in Figure 5-8. In Figure 5-10 two possible autoignition points are indicated. In reality only the left most point is actually associated with a reaction rate integral value of one. The right most point is, however, very close in value and was therefore also labelled to indicate the possibility of an alternative autoignition point.

Comparison of CFD and IQT™ autoignition delays

The CFD autoignition prediction was found to be in good agreement with the measured autoignition delay in the IQT™ and the comparison is shown in Table 5-3 for n-heptane. iso-Octane was also modelled in order to supplement the n-heptane data and the results are shown in Table 5-4.

Modelling and testing was also performed at 12 bar and the results are shown along side those at the standard operating pressure of 21.37 bar.

Table 5-3. Comparison of CFD and measured IQT™ autoignition delay (n-heptane).

Test Point (22 bar)	**IQT™ ID (ms)**	**CFD ID (ms)**
STD T	**3.77**	3.15
STD T – 50	**5.45**	5.05
STD T – 100	**8.65**	10.10
STD T - 150	**21.54**	29.70
Test Point (12 bar)	**IQT™ ID (ms)**	**CFD ID (ms)**
STD T	**5.76**	5.00
STD T – 50	**7.71**	7.20
STD T – 100	**12.14**	12.80
STD T – 150	**20.29**	29.75

Table 5-4. Comparison of CFD and measured IQT™ autoignition delay (iso-octane).

Test Point (22 bar)	**IQT™ ID (ms)**	**CFD ID (ms)**
STD T	**17.32**	18.50
STD T – 50	**25.57**	23.25
STD T – 100	**55.91**	41.40
Test Point (12 bar)	**IQT™ ID (ms)**	**CFD ID (ms)**
STD T	**51.14**	40.40
STD T – 50	**60.24**	49.70
STD T – 100	**67.29**	70.80

The results are shown graphically in Figure 5-12 bellow[v]

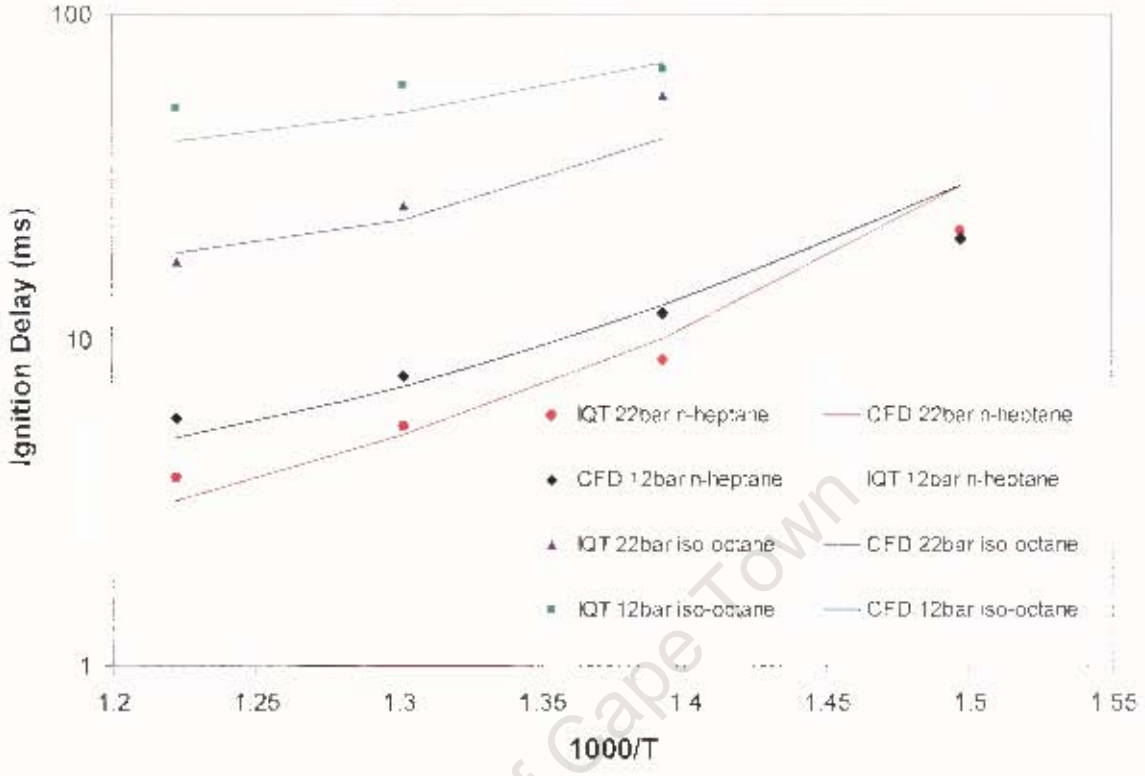

Figure 5-12. Comparison of CFD and measured IQT™ autoignition delay.

The remainder of the results presented here will be limited to modelling at high pressure, as this is the reference operating condition in the IQT™ and more closely related to the conditions in the ASTM D613.

Predicted high-temperature autoignition behaviour

The CFD model was used to predict the autoignition behaviour of n-heptane and iso-octane at temperatures above the safe operating limit of the IQT™. The results are shown in Figure 5-13.

[v] Error bars were considered for the IQT™ data in this graph but the standard deviation is negligibly small (0.05ms for n-heptane) and would be invisible on the log scale.

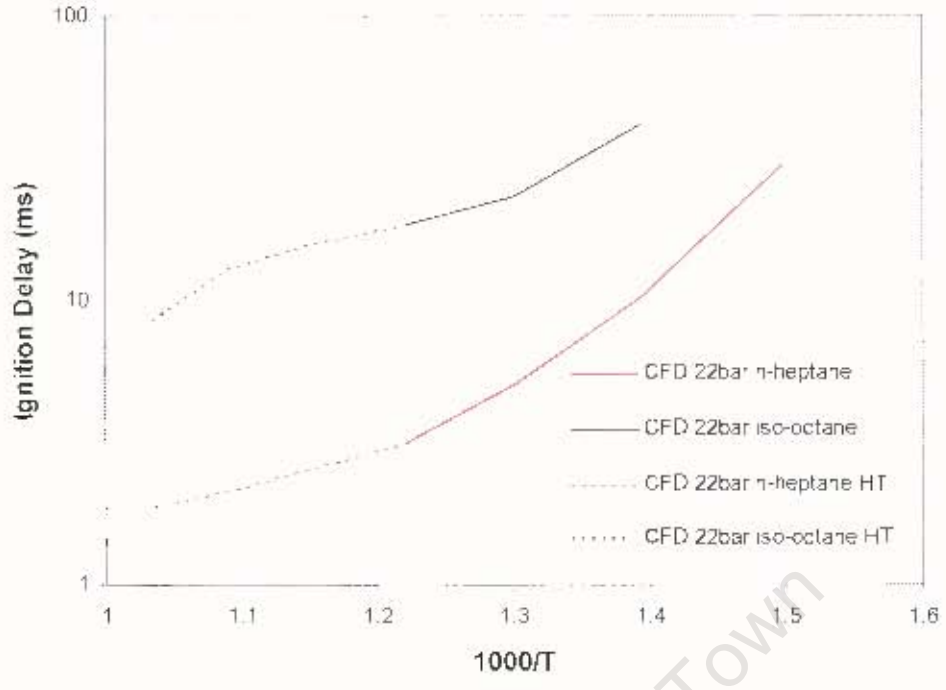

Figure 5-13. Predicted high-temperature autoignition behaviour of n-heptane and iso-octane in the IQT™.

Comparison of CFD and IQT™ autoignition delays for 1-Hexene

In order to further test the capabilities of the CFD model a third fuel, 1-Hexene, was tested. Unlike iso-octane and n-heptane however, the chemical reaction mechanism used for detailed chemical kinetic modelling of 1-hexene, is not strongly backed by literature data. For this reason the coefficients derived for 1-hexene cannot be used with as much confidence as those of n-heptane and iso-octane, and the results of the 1-hexene CFD modelling are presented separately here.

Table 5-5. Comparison of CFD and measured IQT™ autoignition delay (1-hexene).

Test Point (22 bar)	IQT™ ID (ms)	CFD ID (ms)
STD T	**9.03**	9.00
STD T – 50	**13.81**	11.20
STD T – 100	**25.87**	16.40
STD T - 150	**59.05**	30.70

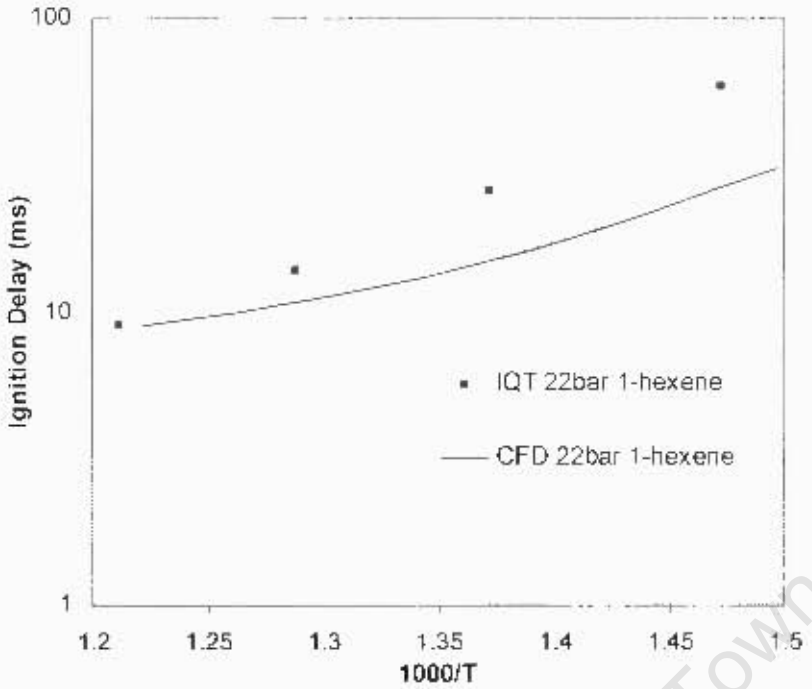

Figure 5-14. Comparison of CFD and measured IQT™ autoignition delay for 1-hexene.

5.3 Inert Particle Output Data

By appropriate choice of the inert particle injection timing it was possible to observe the history of the fuel that ended up near the point of autoignition. at the time of autoignition. Figure 5-15 shows a plot of the recorded *x* and *y* coordinate history of the inert particle for a model of n-heptane at STD T - 100. The particle starts near the origin and moves along the path indicated by the arrows.

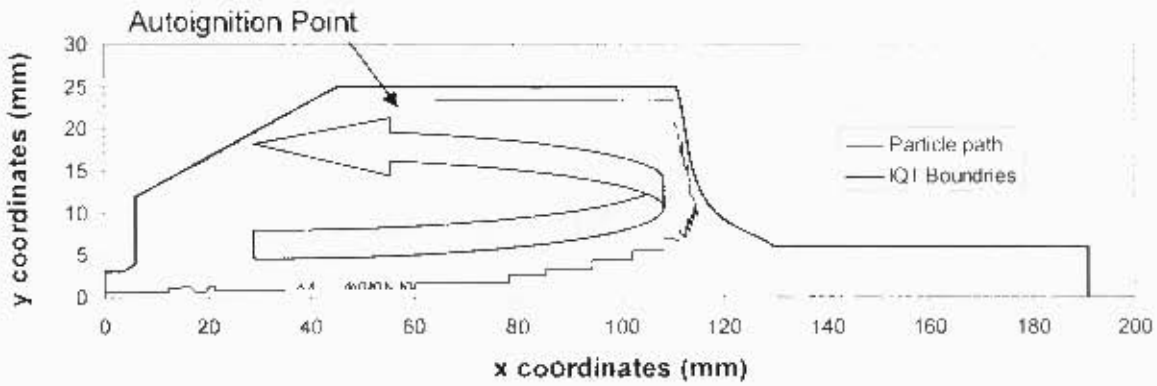

Figure 5-15. Particle trajectory with an arrow indicating increasing time (Note: the trajectory in this example is of a particle at STD T – 100).

This allowed the temperature and fuel/air equivalence ratio histories, recorded for the inert particle, to be confidently used as a reasonable representation of the experience of the autoignition initiating fuel molecule. Figures 5-16 and 5-17 show the inert particle temperature and fuel/air equivalence ratio histories for each of the test points.

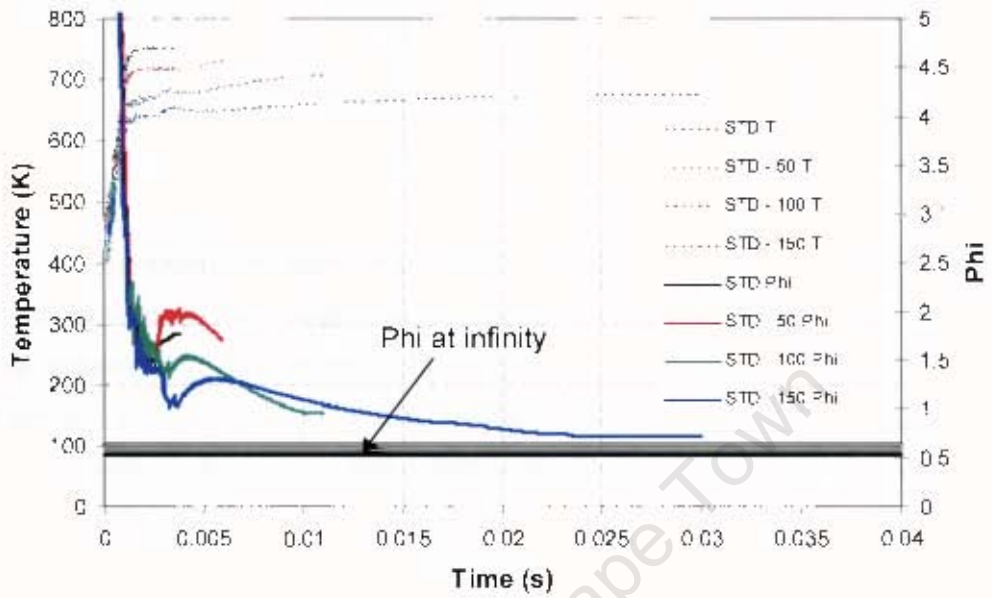

Figure 5-16. Particle temperature and fuel/air equivalence ratio (phi) for n-heptane at various test points.

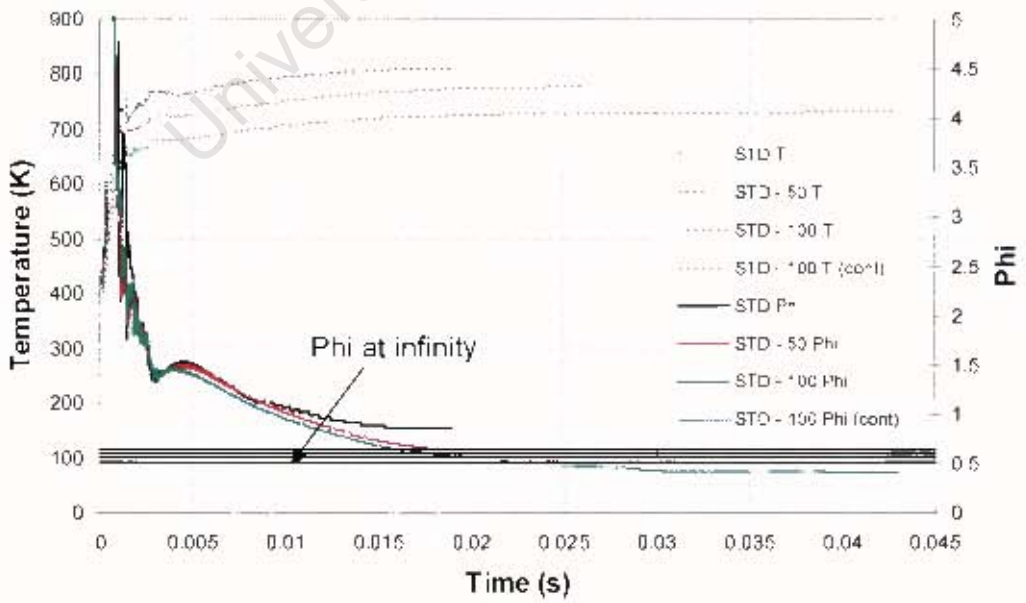

Figure 5-17. Particle temperature and fuel/air equivalence ratio (phi) for iso-octane at various test points.

6 Analysis and Discussion of Results

This section takes a closer look at the results presented in Chapter 5. The intention is to analyse the results of the project in order to offer some useful interpretation. This section will also discuss the shortcomings of the methodology in order to identify areas where future improvements may be made.

As with the previous chapter, the results are handled in a linear fashion, and in the following order:

- IQT™ temperature profile.
- CFD autoignition modelling.
- Inert particle output data.

6.1 IQT™ Temperature Profile

The temperature measurements showed a high level of temperature variation along the length of the axis of the IQT™, with temperatures ranging from relatively cool at the injection nozzle to above the reported test temperature around the middle of the combustion chamber.

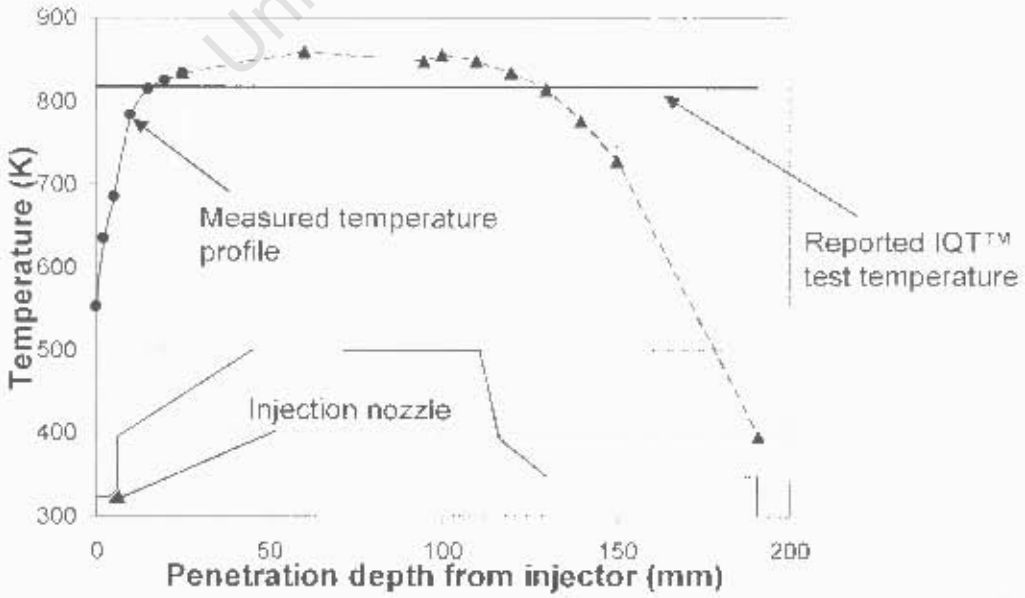

Figure 6-1. Typical temperature profile in the IQT™.

This is borne out in the data collected from the inert particle, with the temperature rising rapidly at first and then continuing to gradually climb. The important thing to note is that the temperature experienced by the fuel is always changing. This would be due in part to heating and evaporation of the fuel, but it is obviously important that changes in the ambient temperature surrounding the fuel were also accounted for by an accurate description of the initial temperature profile.

6.2 CFD Autoignition Modelling

The primary focus of this analysis will be the results of n-heptane and iso-octane at the operating points for which measure IQT™ autoignition data is available. Some brief discussion will, however, be given to the results for 1-hexene, as well as those for the hypothetical high temperature simulations.

n-Heptane and iso-octane

While the CFD model was successful in achieving good agreement between modelled and measured results, it is clear from Figure 6-2 that divergence begins to occur at very long autoignition delays.

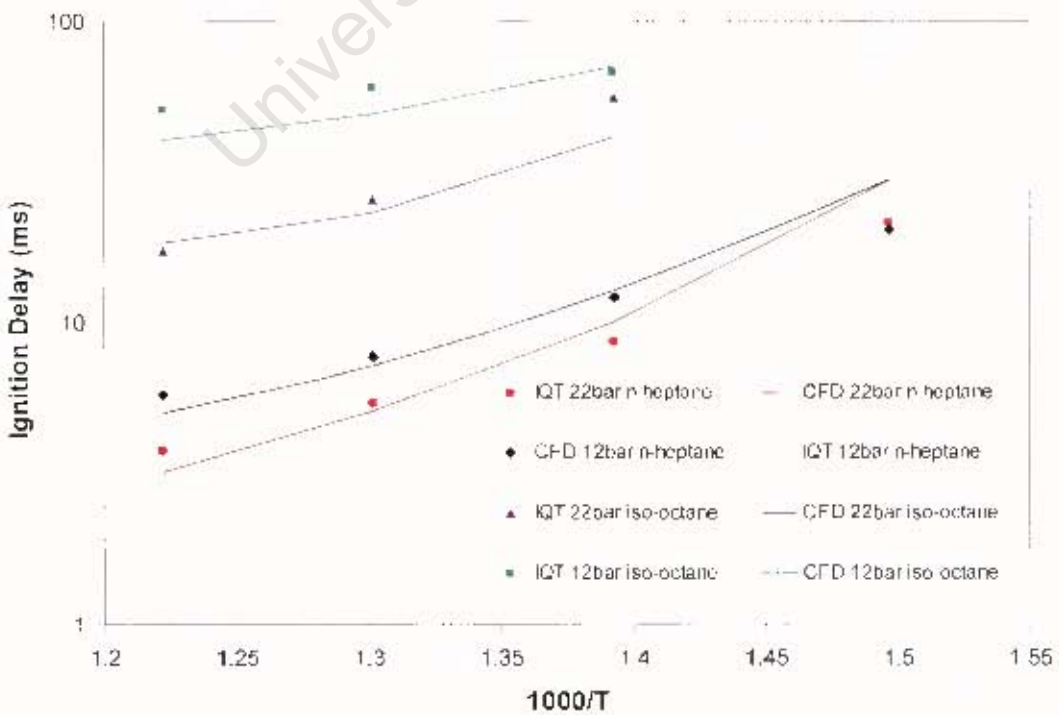

Figure 6-2. Comparison of CFD and measured IQT autoignition delay.

There are many possibilities for this divergence. The following aspects of the model were considered most likely to cause divergence:

- **Accuracy of the Yates model:** Although the Yates model, either new or old, is capable of accurately describing the autoignition behaviour of a fuel, it can only do so if the data to which it is fitted is also accurate. It is essential that the autoignition testing or modelling, used as source data for the Yates model, be accurate if the correct model coefficients are desired.

  Fortunately there is a wealth of data for n-heptane, the primary focus of this project, which is considered to be reliable. The same is true for iso-octane. Of the fuels considered in this work, it is only 1-hexene for which there is a relative lack of confidence in the source data.

- **Application of the Yates model:** Another possible explanation is the manner in which the Yates model is applied to the CFD model. The convective nature of the reaction rate integral, as used in the CFD model, is such that the value in each cell, at a given time step, will be a summation of the incremental value in the cell itself and the weighted average of the additions from neighbouring cells.

  This is at odds with the discrete nature of the autoignition reaction route; in reality the progress of a particular reaction would not be reversed or accelerated by entering space occupied by a reaction further from or closer to autoignition. This is, however, the effect of averaging the values of the reaction rate integral entering a cell.

  To asses the extent to which this flaw impacted the overall accuracy of the CFD model, the reaction rate integral was performed on the inert particle output data and compared to the value given by the CFD model in cells surrounding the inert particle. This is a direct comparison of a discrete treatment of the reaction rate integral and the convective treatment used in the CFD model. The results of the comparison are shown in Figure 6-3.

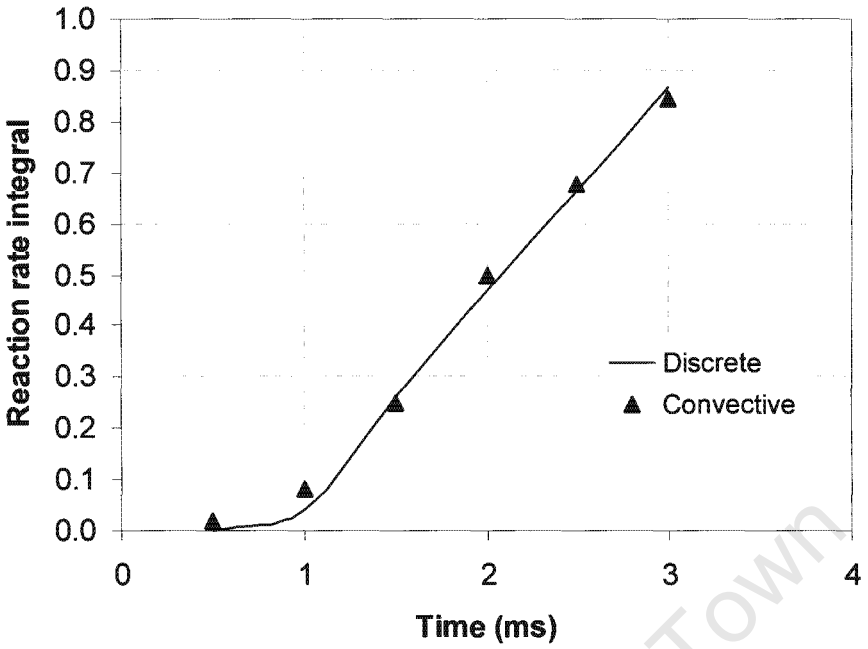

Figure 6-3. Comparison between convective and discrete treatment of the reaction rate integral.

It was found that the progress of the reaction rate integral calculated for the discrete particle closely matched the progress of the reaction rate integral predicted by the CFD model. For this reason it was concluded that the application of the Yates model, as carried out in this study, could in fact be used to confidently predict autoignition delay, and was not the cause of the divergence between modelled and measured results at low temperatures.

- **Value of the equivalence ratio correction factor:** Another possible cause of divergence could be the value of the fuel/air equivalence ratio correction factor (k in Equation 2-24). This factor has a different effect on longer autoignition delays than it does on shorter autoignition delays. This is due to the fact that the average fuel/air ratio experienced by the fuel decreases as the autoignition delay is increased. A different value of k may change the slope of the model results shown in Figure 6-2, bringing them in-line with IQT™ data at low temperatures.

  Swarts (2006) derived a value of -0.46 for k from literature data, giving credence to the idea of a value other than -0.77. The relative effect on autoignition delay, of these two values, is shown in Figure 6-4.

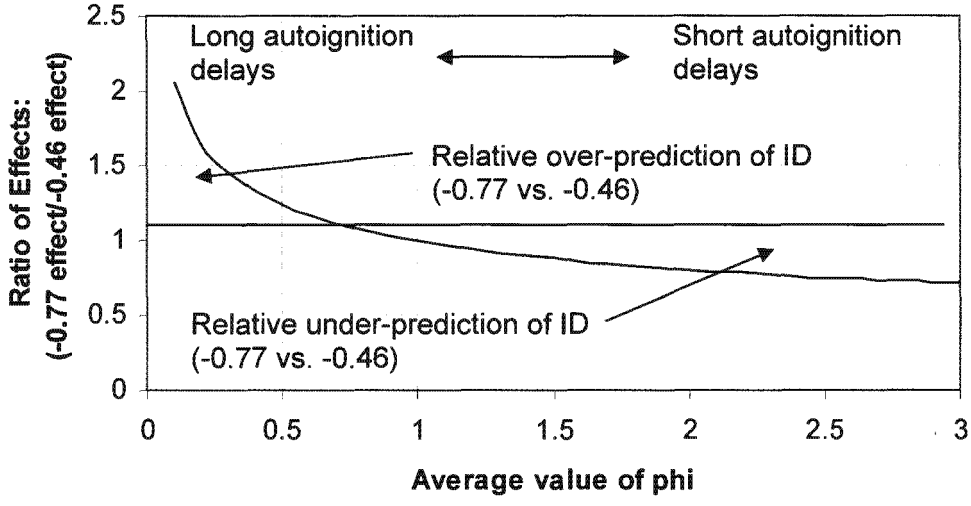

Figure 6-4. Relative effect of two different values of k on autoignition delay.

Figure 6-4 shows, for example, that for an average fuel/air equivalence ratio (phi) of 0.5, a value of -0.77 for k will yield an autoignition delay 1.25 times longer than if a value of -0.46 was used for k. If, however, the average value of phi is less than one, then using -0.77 for k will yield a relatively shorter autoignition delay.

In order to determine the effect of varying the value of k, a sensitivity study was done where the value of k was changed, and the autoignition of n-heptane at standard pressure was remodelled. A comparison between the autoignition predictions for two values of k is shown in Table 6-1 and Figure 6-5. It is clear that the -0.46 value for k had the predicted effect on the CFD results; increasing high temperature autoignition delay predictions and decreasing those at low temperature. While some divergence remains at low temperature, the CFD autoignition prediction is improved at both ends of the temperature range.

Table 6-1. Comparison between CFD results for two values of k (n-heptane at 22 bar).

Test Point (22 bar)	IQT™ ID (ms)	CFD ID -0.77 (ms)	CFD ID -0.46 (ms)
STD T	**3.77**	3.2	3.7
STD T – 50	**5.40**	5.1	5.4
STD T – 100	**8.65**	10.1	9.4
STD T - 150	**21.54**	29.7	25.8

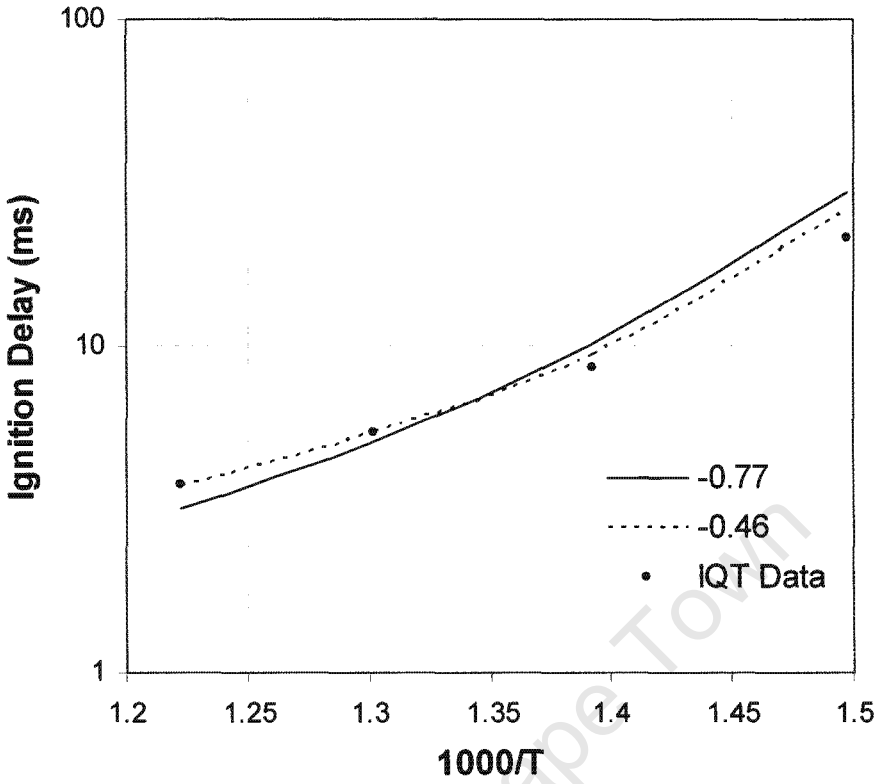

Figure 6-5. Comparison between CFD results for two values of *k* (n-heptane at 22 bar).

It is important to note that, due to the limited availability of fuel data, these numbers are based on a narrow range of fuel/air equivalence ratios. The large range of fuel/air equivalence ratios experienced in very heterogeneous conditions, such as those in the IQT™, makes the universal applicability of these numbers questionable. Furthermore, a study by Fish et al. (1969) found that equivalence ratio had different effects on the pre-cool flame component of the autoignition delay (τ_1 in Equation 2-16) and the post-cool flame component of the autoignition delay (τ_2 in Equation 2-16). This suggests that the fuel/air equivalence ratio correction factor (k) would need to have a different value for long autoignition delays - where the pre-cool flame component dominates - and short autoignition delays - where the influence of the post cool flame component increases.

One possible solution would be to expand the range over which the numbers are applicable by deriving them from a wider range of data. This would, however, require a considerable amount of autoignition testing, which falls outside of the scope of this project.

- **Increased sensitivity:** As the temperature is lowered or the ignition delay is increased, the model becomes more sensitive to inaccuracies.

  As the mean operating temperature is lowered, the effect of small temperature inaccuracies becomes increasingly significant. Temperature inaccuracies are inevitable, and arise from measuring inaccuracies in the initial temperature profile, and imperfect treatment of vaporisation, boiling and heat transfer in the CFD code.

  The same imperfect treatment also results in compounded errors, where errors grow due to the deterioration of the accuracy of the initial data at every time step. For short autoignition delays the compounded error will not have reached a point where it significantly contributes to the results, but for very long autoignition delays it is possible that the errors will have compounded to a point where it is unlikely that the model will be capable of effectively simulating reality.

  This phenomenon can be seen in the difference in accuracy between the CFD results for n-heptane and iso-octane. The results for n-heptane are consistently better than those for iso-octane, and the level of accuracy of the n-heptane model suggests that the temperature and other variables must be fairly accurately initialised. The main difference between modelling n-heptane and iso-octane is the number of time steps required. For example, at STD T and 22 bar an n-heptane model requires approximately 3800 time steps, whereas at the same test point an iso-octane model requires approximately 18000 time steps.

  Although the divergence shown in Figure 6-2 would become more significant were the test temperatures even lower, or the autoignition delays longer, the modelled autoignition delays within the ranges treated in this study are still considered to be in good agreement with the measured autoignition delays in the IQT™.

1-Hexene

While the results of the CFD model for n-heptane and iso-octane show promise, those for 1-hexene diverged from the IQT™ data the moment the test point was lowered below STD T (see Figure 5-14). While it is probable that the 1-hexene model was subject to the same limitations (discussed above) as the models for n-heptane and iso-octane, the divergence between the modelled and measured autoignition delays is more severe in this case.

The main difference between 1-hexene, and the other two fuels, is the lack of literature data to substantiate the mechanisms used for the detailed chemical kinetic model. As the coefficients used for the CFD model of the IQT™ are derived from the results of the detailed chemical kinetics this is a potentially fundamental limitation.

The lack of agreement between the modelled and measured autoignition delays for 1-hexene by itself could point to a severe case of one of the modelling limitations dealt with previously. But the fact that this lack of agreement is in contrast to the good agreement found in the modelling of the other fuels, suggests that the cause must be the underlying chemical characterisation of 1-hexene.

6.3 *Inert Particle Output Data*

It was possible to time the injection of the inert particle so that it ended up near the point of autoignition, at the time of autoignition. Furthermore, as shown in Figure 6-3, the data collected for the history of the inert particle was used to calculate reaction progress that compared well with the reaction progress predicted by the CFD model. For this reason it is reasonable to assume that the conditions observed and tracked by the inert particle are a fair representation of the history of the fuel that initiated autoignition.

A typical inert particle history is shown in Figure 6-6. The history is for a simulation of n-heptane autoignition at STD T – 150 and, while not identical to data at other test points, is useful for highlighting trends seen in all of the particle histories.

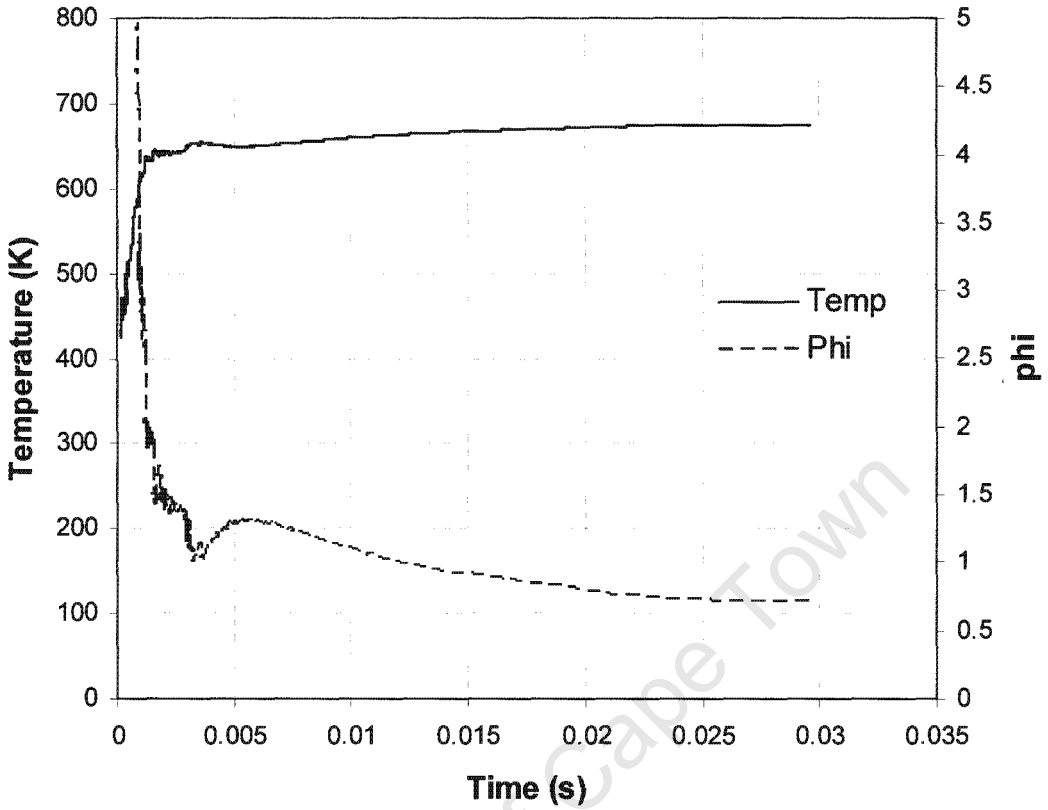

Figure 6-6. Representative particle history (n-heptane at STD T - 150)

It is clear from Figure 6-6 that the fuel experiences a very wide range of temperatures and fuel/air equivalence ratios. In fact the conditions experienced by the fuel are constantly varying and by extension so is the instantaneous autoignition delay. The temperature rises rapidly at first and then continues to climb smoothly. The fuel/air equivalence ratio, on the other hand, displays the opposite behaviour; with very high initial values that drop off rapidly at first and then continue to decline.

Of interest is the fact that while increasing temperature would tend to decrease the autoignition delay, the decreasing fuel/air equivalence ratio will have a counteracting effect via Equation 6-1.

$$\tau = \tau_{\phi=1} . \phi^{k} \qquad \text{(Eq 6-1)}$$

Where $\tau_{\phi=1}$ is the value of the autoignition delay under stoichiometric conditions, ϕ is the fuel/air equivalence ratio and k is the fuel/air equivalence ratio correction factor.

At about 3ms the temperature curve exhibits a slight "bump" where the temperature rises more rapidly and then drops down again. This is accompanied by a more noticeable dip in the fuel/air equivalence ratio curve.

These anomalies in the particle history coincide with the point at which the particle suddenly changes direction and moves up along the wall of the IQT™. The temperature rise is due to the fact that the particle is doubling back into a hotter area, while the more significant drop in fuel/air equivalence ratio is due to the particle leaving an area where fuel has amassed at the entrance to the port leading to the pressure transducer. This rich zone is indicated in Figure 6-7.

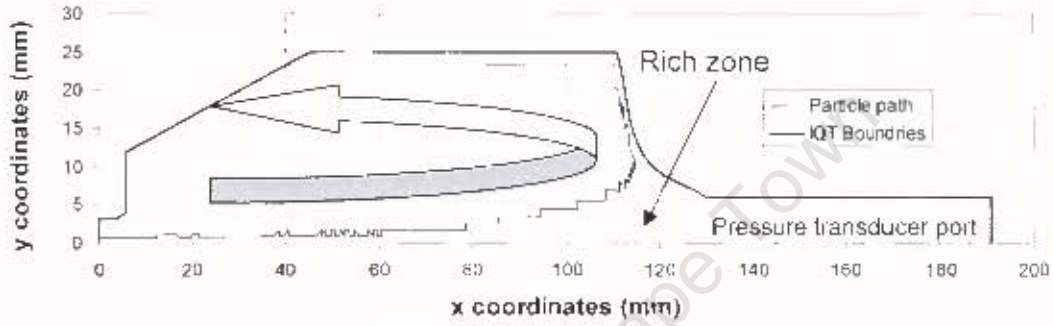

Figure 6-7. Inert particle trajectory, indicating rich zone at the entrance to the pressure transducer port.

It is also interesting to note that as the test temperature was reduced, so was the value of the fuel/air equivalence ratio at any given time. This phenomenon is illustrated in Figure 6-8.

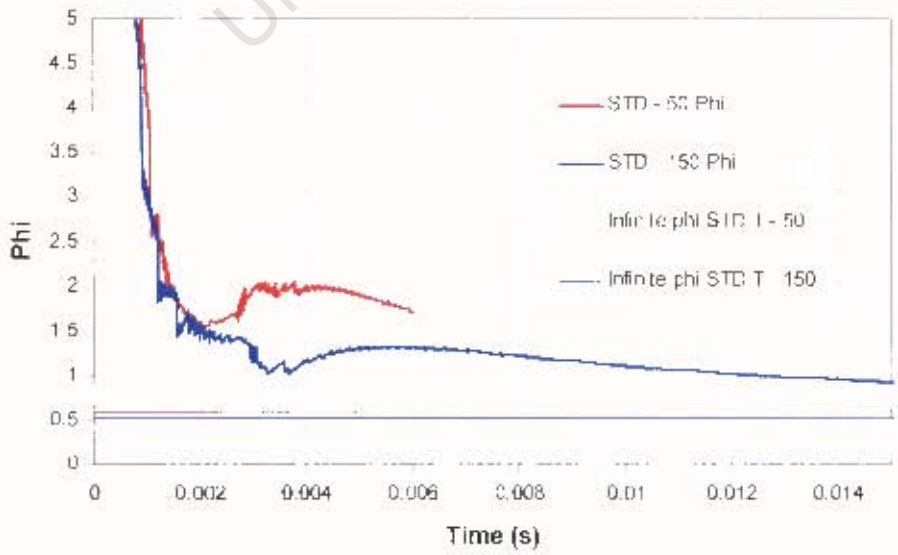

Figure 6-8. Comparison of the fuel/air equivalence ratio histories for different test conditions.

As an example, in Figure 6-8 the value of the equivalence ratio at 4ms is about 2 for the STD – 50 history, whereas for the STD T – 150 history the value is closer to 1.25 at the same time.

There are a couple of likely causes for this difference in behaviour at different test conditions. The first is that at higher test temperatures more liquid fuel has evaporated and entered the mixture phase in which the fuel/air ratio is calculated.

The second is that at higher test temperatures there is less air in the combustion chamber than at lower temperatures. This is due to the lower density of the air at high temperatures and means that, given enough time for a homogenous mixture to form, the fuel/air equivalence ratio would be higher at high temperature than at low temperatures.

This "long-term" fuel/air equivalence ratio is indicated in Figure 6-8 by the fine horizontal lines labelled "infinite phi". They were given this name as they represent the value of phi after a very long or infinite amount of time. The values of the "infinite" fuel/air equivalence ratio are shown in Figure 6-9 for a range of reported IQT™ test temperatures.

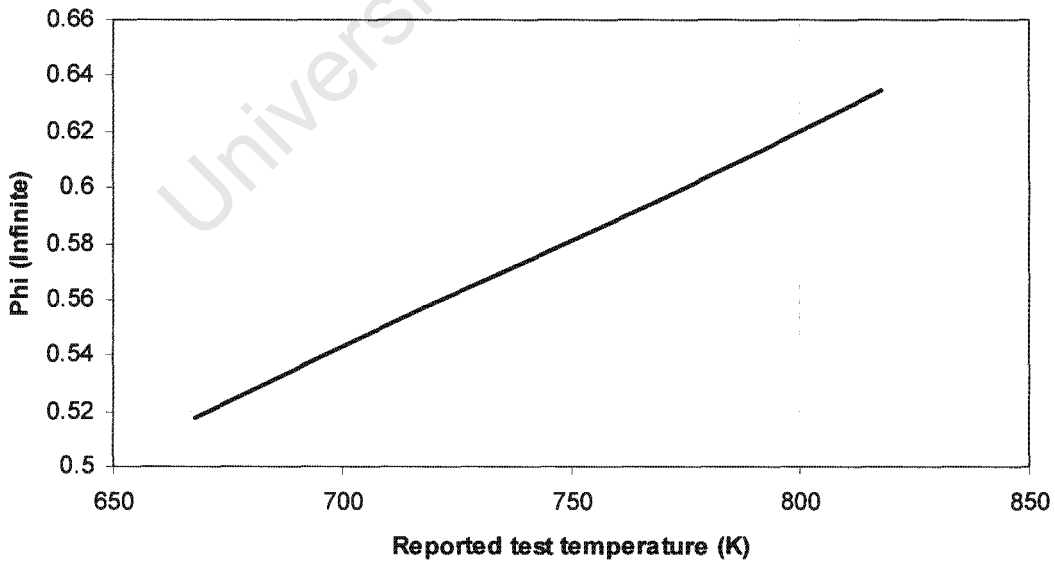

Figure 6-9. "Infinite" fuel/air equivalence ratio for a range of reported IQT™ test temperatures (at 22 bar).

Significance of the data

This data can be used to further understand the chemical reaction history of the autoignition of fuels in the IQT™ outside of the CFD environment, taking into account the temperature and fuel/air equivalence ratio history. This is done by reducing the complex problem posed by the heterogeneous nature of the IQT™, to a set of columns of data. This in turn enables the generation of plots, such as the one in Figure 6-6, for visual analysis. Visualization is immensely powerful as trends, and relationships between variables in a complex problem, often emerge more clearly when the problem can be visualised.

Beyond the benefits of visualisation, there is also the advantage of using Excel® tools to extract mathematical descriptions of various phenomena. This is essential if it is desirable to reconcile the discrepancies between autoignition behaviour in the IQT™, and intrinsic chemical autoignition behaviour, with a simple modification to the Yates model. It is in this way that Yates et al. (2007) made successful use of the fuel history data generated by this project to develop an improved understanding of the relationship between autoignition delay data fro the IQT™, and cetane number in the ASTM D613.

7 Conclusions

Based on the results and discussion of the previous chapter, the following conclusions were drawn:

- Initial modelling of the heating procedure of the IQT™ reinforced the idea that a heterogeneous temperature profile existed within the IQT™ combustion chamber. The modelled profile was found to be in good qualitative agreement with the profile that was ultimately measured.

- It was found that the temperature in the IQT™ is not homogeneous, and therefore the reported test temperature is not sufficient to describe the temperatures experienced by fuel injected into the combustion chamber when applying an autoignition delay model.

- The technique of using CFD modelling of fuel injection - to resolve spatial and temporal details of fuel history - in conjunction with the Yates model for autoignition delay, produced good agreement with experimental autoignition delay data from the IQT™. There are, however, conditions for which the model is best suited and they are as follows:

    - Short autoignition delays associated with high temperatures in the IQT™ and high cetane number fuels.
    - Fuels for which there is confidence in the chemical mechanism used for the detailed chemical kinetics, from which the coefficient for the Yates model are derived.

- In this application a value other than -0.77 may be more appropriate for the fuel/air equivalence correction factor (k). Swarts (2006) derived a value of -0.46, from literature data, that showed a significant improvement in the results for n-heptane at 22 bar. Despite the evident improvement in the results it is important to note that the value derived by Swarts was based on a limited range of data. It is also unclear, given the observations of Fish et al. (1969), whether a single value is appropriate for all operating conditions.

- It was possible to create a new injection consisting of a small, inert, observation particle that responded to the fluid flow in the same way as the mixture surrounding it, without taking part in any phase change or heat transfer processes. By appropriate timing of the injection it was possible to ensure that the inert particle tracked the fuel and ended up near the point of autoignition, at the time of autoignition.

- The inert particle could be used as an observation tool, recording the conditions in the computational cell surrounding it at every time step.

- The progress of the reaction rate integral based on the inert particle output data closely matched that of the reaction rate integral calculated by the CFD model.

- Due to the fact that the inert particle travelled along approximately the same physical path as the fuel that initiated autoignition, and the fact that the reaction rate integral calculated based on its output data matched that of the CFD model, it was concluded that the history defined by the inert particle output data is representative of the autoignition initiating fuel.

- This data can be used to further understand the chemical reaction history of the autoignition of fuels in the IQT™ outside of the CFD environment, taking into account the temperature and fuel/air equivalence ratio history.

8 Recommendations

While the demonstrated technique was successful in producing data that is believed to be representative of the conditions experienced by a fuel in the IQT™, the following recommendations are made to ensure that the results can be used with confidence:

- It is best to use the method of autoignition delay prediction, proposed in this report, for shorter autoignition delays and higher temperatures.

- In order to ensure accurate results for autoignition delay prediction, it is important to ensure that there is confidence in the data used to derive the coefficients for the Yates model.

- The sensitivity of the model to the fuel/air equivalence correction factor (k) should be evaluated for other test conditions and fuels.

- The value of the fuel/air equivalence correction factor (k) should be investigated over a wide range of temperatures and fuel/air equivalence ratios. Given a wider range of data a value may be found that could be applied universally with more confidence. It may in fact be more accurate to have a variable value that is a function of the mean test temperature. This would enable a better description of the varying effects of equivalence ratio on the pre and post cool flame components of the autoignition delay, as observed by Fish et al. (1969).

- Further study should be carried out to determine the effects of varying the injection parameters. This could provide valuable insight into the effect of injection pressure, atomization and spray structure on the autoignition delay behaviour of fuels.

- The possibility of adding optical access to the IQT™ should be investigated. This could provide validation of the spray behaviour as predicted by the CFD modelling, as well as experimental data regarding the location of the point of autoignition.

- A wider rage of IQT™ data would be useful to determine the exact applicability of the demonstrated technique with regards to pressure, temperature and fuel type.

- The possibility of extending the technique to include heat release to simulate cool flame reactions should be investigated. If the cool flame heat release could be directly implemented into the model, rather than indirectly via an empirically determined temperature rise (ΔT in Equation 2-19), then the resultant pressure rise could be simulated. Any reduction in the effect of the cool flame heat release due to the heterogeneous, non-adiabatic nature of the spray simulation would be automatically simulated.

9 References

"AET Procedures Manual: Ignition Quality Tester (IQT™) for Diesel Fuel Cetane Number Evaluation", 8.3, Advanced Engine Technology (AET), August 2003

Ahmadi-Befrui B., Wiesler B., Winklhofer E., "The Propagation of Fuel Sprays in a Research Diesel Engine – A Joint Numerical and Experimental Analysis", SAE 910181, 1991

Ali A., Cazzoli G., Kong S., Reitz R. D., Montgomery C. J., "Improvement in Computational Efficiency for HCCI Engine Modeling by Using Reduced Mechanisms and Parallel Computing", Engine Research Center, University of Wisconsin-Madison and Reaction Engineering International, 2003

Allard L. N., Webster G. D., Hole N. J., Ryan III T. W., Otto D., Fairbridge C. W., "Diesel Fuel Ignition Quality as Determined in the Ignition Quality Tester (IQT™)", SAE 961182, 1996

Allard L. N., Webster G. D., Hole N. J., Ryan T. W., Bker G., Beregszaszy A., Fairbridge C. W., Ecker A., Rath J., "Analysis of the Ignition Behavior of the ASTM D-613 Primary Reference Fuels and Full Boiling Rage Diesel Fuels in the Ignition Quality Tester (IQT™) – Part III", SAE 1999-01-3591, 1999

Araldi A. A., Ryan III T. W., "Cetane Effects on Diesel Ignition Delay Times Measured in a Constant Volume Combustion Apparatus", SAE 952352, 1995

ASTM Method D613-03b, "Standard Test Method for Cetane Number of Diesel Fuel Oil", ASTM, August 2003

ASTM Method D6890-03, "Standard Test Method for Determination of Ignition Delay and Derived Cetane Number (DCN) of Diesel Fuel Oils by Combustion in a Constant Volume Chamber", ASTM, August 2003

Barroso G., Schneider B., Boulouchos K., "An Extensive Parametric Study on Diesel Spray Simulation and Verification with Experimental Data", SAE 2003-01-3230, 2003

Cox R., "The Development of an Autoignition Sub-model for use in CFD Combustion Simulations", MSc Thesis, University of Cape Town, 2006

Curran, H. J., Gaffuri, P., Pitz, W. J., Westbrook, C. K., "A Comprehensive Modeling Study of n-Heptane Oxidation", Combust. Flame, Vol. 114, p 149-177, 1998

Curran, H. J., Gaffuri, P., Pitz, W. J., Westbrook, C. K., "A Comprehensive Modeling Study of iso-Octane Oxidation", Combust. Flame, Vol. 129, p 253-280, 2002

Dec J. E., "A Conceptual Model of DI Diesel Combustion Based on Laser-Sheet Imaging", SAE 970873, 1997

Douaud A. M., Eyzat P., "Four Octane Number Method for Prediction the Anti-Knock Behaviour of Fuels and Engines", SAE 780080, 1987

Fish A., Read I. A., Affleck W. S., Haskell W. W., "The Controlling Role of Cool Flames in Two-Stage Ignition", The Journal of the Combustion Institute, vol. 13, 1969

"Fluent 6.2 Documentation: User Guide and UDF Manual", Fluent Inc.

Gustavsson J., Golovitchev V. I., Helmantel A., "3-D Modeling of Conventional and HCCI Combustion Diesel Engines", SAE 04FFL-130, 2004

International Organization for Standardization (ISO) "Diesel engines – Calibrating nozzle, delay pintle type", ISO 4010:1998(E), 1998

Livengood J. C., Wu P. C., "Correlation of Autoignition Phenomena in Internal Combustion Engines and Rapid Compression Machines". 5th Symp. (Int.) on Combustion, p. 347, Reinhold Publishing Corp, 1955

Londleni S. C., "A Theoretical Assessment of Fuel Combustion Attributes to Enhance the Operational Envelope of HCCI Engines", MSc Thesis, University of Cape Town, 2006

National Institute of Standards and Technology (NIST), WebBook, [Online], Available: http://webbook.nist.gov/cgi/fluid.cgi?ID=C142825&Action=Page

Rose J. W., Cooper J. R., "Technical Data on Fuel", 7th ed, p. 273-275 & p. 281 Scottish Academic Press, 1977

Swarts A., "Insights Relating to Octane Rating and the Underlying Role of Autoignition", PhD thesis, University of Cape Town, 2006

Tao F., Golovitchev V. I., Chomiak J., "Numerical Modeling of Auto-Ignition, Combustion and Soot Formation for n-Heptane Sprays in a High Pressure Constant-Volume Chamber", Department of Thermo and Fluid Dynamics Chalmers University of Technology, 1999

Tao F., Golovitchev V. I., Chomiak J., "Self-Ignition and Early Combustion Process of n-Heptane Sprays Under Diluted Air Conditions: Numerical Studies Based on Detailed Chemistry", SAE 200-01-2931, 2000

Tao F., Chomiak J., "Numerical Investigation of Reaction Zone Structure and Flame Liftoff of DI Diesel Sprays with Complex Chemistry", SAE 2002-01-1114, 2002

Versteeg H. K., Malalasekera W., "An Introduction to Computational Fluid Dynamics: The Finite Volume Method", Pearson Prentice Hall, Longman Group Ltd, 1995

Viljoen, C. L., Yates, A. D. B., Swarts, A., "An Investigation of the Ignition Delay Character of Different Fuel Components and an Assessment of Various Autoignition Modelling Approaches", SAE 2005-01-2084, 2005

Viljoen C. L., Yates A. D. B., Coetzer R. J. L., "A Molecular Modelling Investigation of Selected Gasoline Molecules to Relate Oxidation Pathways to their Autoignition Behaviour", SAE 2007-01-0005, 2007

Westbrook, C. K., Curran, H.J., Pitz, W. J., Griffiths, J. F., Mohamed, C., Wo, S. K., "The Effects of Pressure, Temperature and Combustion on the Reactivity of Alkanes: Experiments and Modeling in a Rapid Compression Machine", Twenty-seventh Symposium (Int.) on Combustion, The Combustion Institute, p. 371-378, 1998

Yates A. D. B., Viljoen C. L., Swarts A., "Understanding the Relationship Between Cetane Number and Combustion Bomb Ignition Delay Measurements", SAE 2004-01-2017, 2004

Yates A. D. B., Viljoen C., Metcalf O., "An Accurate Determination of the Cetane Number of Sasol GTL Diesel", SAE 2007-01-0026, 2007

Appendix 1 - UDF Code

User Defined Functions (UDFs) are used to perform two vital tasks in this project. The first task was to define a User Defined Scalar (UDS) that represents the instantaneous reaction rate, and the second task was to record the changing conditions around the inert particle.

The UDFs in this section have the following basic structure:

- **Include standard FLUENT® libraries:** This allows the use of various standard instructions, the definitions of which are contained within the libraries.

- **Define UDF Type:** Here the user specifies the type of UDF to be used. Different types of UDFs have different applications and therefore must be chosen carefully for a particular task.

- **Define variables to be used:** Here the user specifies a list of variables that will be used in the remainder of the code.

- **Specify or acquire domain, thread and cell data:** Here the user tells the programme where (in the domain) to perform the calculations.

- **List of instructions:** This is where the instructions and calculations are performed.

The code used for each UDF is included on the following pages.

Reaction rate UDF

The code for this UDF was originally written by Cox (2006) for an early version of the Yates model (Equation 2-14). For the purposes of this project the code was modified to implement the new Yates model (Equation 2-16). The modified code is shown below:

```
                                        UDF - Autoignition Integral.txt
#include "udf.h"

/* ********************** Yates Model Coefficients ********************** */

/* Fill in the values of lnAi, ni, Bi, C0, C1, C2 and m specific to the fuel being modelled */

#define lnA1 -20.01
#define n1 0.125
#define B1 15162
#define lnA2 -11.11
#define n2 -0.975
#define B2 15044
#define C0 2632
#define C1 -1.745
#define C2 1458
#define m  0.045

/* Define the constant volume/constan pressure correction value */

#define Gamma 1.15

/* air fuel ratio  data, input the stoichiometric fuel/air ratio and the fuel/air
   equivalence ratio correction factor (for n heptane stoich = 0.065907) */

#define stoich 0.065907
#define k -0.774747

DEFINE_SOURCE(ignitioninregral,c,t,dS,eqn)
{

        real p_operating = RP_Get_Real ("operating-pressure");
        real dp = C_P(c,t) + p_operating;
        real dTprime = (C1*C_T(c,t)+C2*pow((dp/101300),m));
        real dT = (dTprime + pow((pow(dTprime,2)-(C0*C1)),0.5))/2;

        if (C_YI(c,t,4) <= 0.05)
        {
                real source = 0;
                dS[eqn] = 0.0;
                return source;
        }

        else if (dp <= 0)

        {
                real source = 0;
                dS[eqn] = 0.0;
                return source;
        }

        else if (C_T(c,t) >= 1500)

        {
                real source = 0;
                dS[eqn] = 0.0;
                return source;
        }

        else
        {


        real phi = ((C_YI(c,t,0))/(C_YI(c,t,4)))/stoich;

        real Arr1 = pow((dp/101300),n1) *
exp(lnA1+B1/C_T(c,t))*(1-exp(-62*dT/Gamma/pow(C_T(c,t),2)));
        real Arr2 = pow((dp/101300),n2) * exp(lnA2+B2/(C_T(c,t)+dT/Gamma));


        real source =  (1000 * C_R(c,t)) / ((Arr1+Arr2)*pow(phi,k)); /*this is the User Defined
Scalar
                                                                      that will be integrated by
the solver*/
        dS[eqn] = 0.0;
        return source;
        }
}
```

Fuel history tracking UDF

The code was written to observe the values of fuel/air equivalence ratio, pressure, position and temperature of an inert particle travelling in the fluid flow in the IQT™ combustion chamber. This data is then output to a comma separated variables (csv) file for analysis in Excel®. The code is shown below:

```
                                        UDF   History tracking.txt
#include "udf.h"
#include "dpm.h"
#include "surf.h"

#define STOICH 0.065907

DLFINE EXECUTE_AT_END(test)

{
        /*Define variables to be used*/
        real time = CURRENT_TIME;
        real Temp = 0;
        real x[ND_ND];
        real Xpos = 0;
        real Ypos = 0;
        real Pcell;
        real p_operating = RP_Get_Real("operating-pressure");
        real pressure = 0;
        real phi = 0;

        /*Setup domain, thread cell and particle pointers*/
        Domain *d;
        Thread *c_thread;
        cell_t cell;

        Particle *p;
        Injection *I, *IList;

        /*Setup output file*/
        FILE *data;

        /* Get domain ID*/
        d   Get_Domain(1);

        /* Get particle injection list*/
        IList = Get_dpm_injections();

        /* Loop over all the injection*/
        loop(I, IList)

                /* Test if this is the injection you want to work with*/
                if(strcmp("inert" , I->name) == 0)
                {
                        loop(p,I->p)
                        {
                        cell =  P_CELL(p);
                        c_thread = P_CELL_THREAD(p);
                        /* Now get data from the cell as you want */

                                /*Modify particel density to match surroundings */
                                P_RHO(p) = C_R(cell,c_thread);

                                C_CENTROID(x,cell,c_thread);

                                if(x[1] >= Ypos)
                                {
                                Pcell = C_P(cell,c_thread);
                        Temp = C_T(cell,c_thread);
                                Xpos = x[0];
                                Ypos = x[1];
                                pressure = Pcell + p_operating;
                                phi = (C_YI(cell,c_thread,0)/C_YI(cell,c_thread,4))/STOICH;
                                }
                        }
                }

                if(Temp > 0)
                {
                data = fopen("Output.csv","a");

fprintf(data,"%12.6f,%12.5f,%12.5f,%12.2f,%12.3f,%12.3f\n",Time,Xpos,Ypos,Temp,pressure,phi);

                fclose(data);

                }
}
```

Appendix 2 – Yates Model Coefficients

The Following Tables contains the coefficient used in the improved Yates model:

n-Heptane Coefficients	
Coefficient	**Value**
$\ln A_1$	-20.01
n_1	0.125
B_1	15162
$\ln A_2$	-11.11
n_2	-0.975
B_2	15044
C_0	2632
C_1	-1.745
C_2	1458
m	0.045
γ	1.35

1-Hexene Coefficients	
Coefficient	**Value**
$\ln A_1$	-23.32
n_1	-0.077
B_1	17094
$\ln A_2$	-10.13
n_2	-0.944
B_2	14356
C_0	2632
C_1	-1.108
C_2	984
m	0.027
γ	1.35

Iso-Octane Coefficients	
Coefficient	**Value**
$\ln A_1$	-23.21
n_1	-0.146
B_1	18431
$\ln A_2$	-11.47
n_2	-1.081
B_2	15381
C_0	3000
C_1	-1.255
C_2	957
m	0.038
γ	1.35

Appendix 3 – Typical IQT™ Report

The following is a typical IQT™ report for n-heptane:

IQT™ Results - Run Details

Run ID: 682
Fuel ID: N-Heptane
ISS version: 3.40a, rev. 12a
Test Method: ASTM D6890-04

Date & Time: 2006/10/18 05:54:03
Operator: GF
Setpoint: 568.5
S/W License Code: 397F-A525

Inj. #	ID	DCN	Charge P.	Inj. P.	Test T.	Trans. T.	Nozzle T.	Coolant T.	Air B. T.
1	3.807	52.17	2.138	1.205	537.0	137.2	51.8	40.1	590.6
2	3.878	51.21	2.137	1.205	536.9	136.9	51.4	40.3	591.4
3	3.957	50.19	2.139	1.204	537.5	136.4	51.3	40.4	591.7
4	3.937	50.44	2.138	1.203	536.9	136.8	51.5	40.4	590.8
5	3.877	51.21	2.138	1.202	536.4	137.3	51.0	40.2	591.1
6	3.860	51.44	2.139	1.201	536.7	136.9	51.5	40.9	591.7
7	3.825	51.93	2.138	1.200	537.4	137.2	51.7	40.5	590.9
8	3.851	51.57	2.139	1.197	536.7	137.3	50.8	40.3	590.2
9	3.849	51.60	2.139	1.195	537.2	136.9	50.9	40.3	591.8
10	3.783	52.51	2.138	1.191	537.2	137.6	51.5	40.4	591.9
11	3.881	51.17	2.139	1.191	537.1	137.6	50.7	41.0	590.5
12	3.877	51.21	2.139	1.202	537.8	137.4	51.3	40.3	591.5
13	3.885	51.11	2.137	1.209	537.5	137.6	51.3	40.3	592.0
14	3.965	50.09	2.140	1.213	537.0	137.8	50.9	40.6	590.0
15	3.841	51.70	2.137	1.219	536.9	138.0	51.0	40.4	590.8
16	3.822	51.96	2.138	1.216	536.9	137.3	51.1	40.4	591.8
17	3.791	52.40	2.138	1.215	537.8	137.9	51.4	40.2	591.2
18	3.871	51.29	2.139	1.215	536.8	138.1	50.9	40.4	590.8
19	3.848	51.61	2.138	1.211	537.3	137.6	51.0	40.6	591.9
20	3.942	50.37	2.137	1.208	537.4	137.9	51.1	40.5	590.3
21	3.892	51.02	2.139	1.208	536.8	138.3	50.5	40.2	590.0
22	3.788	52.43	2.138	1.207	537.1	138.4	50.9	40.3	591.8
23	3.887	51.09	2.137	1.205	537.2	138.1	51.3	40.6	591.7
24	3.927	50.57	2.138	1.204	537.0	137.6	50.6	40.1	590.4
25	3.866	51.36	2.137	1.205	536.9	137.9	51.0	40.7	591.9
26	3.879	51.20	2.138	1.202	537.3	137.8	51.3	40.1	592.0
27	3.917	50.70	2.140	1.201	537.2	138.0	51.5	40.4	590.7
28	3.952	50.25	2.139	1.201	537.2	138.2	51.5	40.6	591.3
29	3.908	50.81	2.138	1.197	537.3	138.2	51.7	40.5	591.5
30	3.918	50.68	2.139	1.196	536.9	138.5	51.4	40.4	590.2
31	3.946	50.32	2.138	1.193	537.3	138.3	51.3	40.3	591.7
32	3.885	51.11	2.138	1.189	537.1	138.0	51.5	40.5	591.1
Avg.:	3.878	51.20	2.138	1.203	537.1	137.7	51.2	40.4	591.2
Min:	3.783	50.09	2.137	1.189	536.4	136.4	50.5	40.1	590.0
Max:	3.965	52.51	2.140	1.219	537.8	138.5	51.8	41.0	592.0
Range:	0.182	2.42	0.003	0.030	1.4	2.1	1.4	1.0	2.0
Std. Dev.:	0.050	0.67	0.001	0.008	0.3	0.5	0.3	0.2	0.6